

Article

A Multi-Scale Analysis of the Extreme Precipitation in Southern Brazil in April/May 2024

Michelle Simões Reboita ^{1,*}, Enrique Vieira Mattos ¹, Bruno César Capucin ², Diego Oliveira de Souza ³
and Glauber Willian de Souza Ferreira ¹

¹ Natural Resources Institute, Federal University of Itajubá, Av. BPS, 1303, Itajubá 37500-903, MG, Brazil; enrique@unifei.edu.br (E.V.M.); glauber_ferreira@unifei.edu.br (G.W.d.S.F.)

² Ampere Consultoria, Rua Cardeal Arcoverde, 1641, São Paulo 05407-002, SP, Brazil; bruno.capucin@ampereconsultoria.com.br

³ National Center for Monitoring and Early Warning of Natural Disasters, Estrada Doutor Altino Bondesan, 500, São José dos Campos 12247-016, SP, Brazil; diego.souza@cemaden.gov.br

* Correspondence: reboita@unifei.edu.br

Abstract: Since 2020, southern Brazil's Rio Grande do Sul (RS) State has been affected by extreme precipitation episodes caused by different atmospheric systems. However, the most extreme was registered between the end of April and the beginning of May 2024. This extreme precipitation caused floods in most parts of the state, affecting 2,398,255 people and leading to 183 deaths and 27 missing persons. Due to the severity of this episode, we need to understand its drivers. In this context, the main objective of this study is a multi-scale analysis of the extreme precipitation between 26 April and 5 May, i.e., an analysis of the large-scale patterns of the atmosphere, a description of the synoptic environment, and an analysis of the mesoscale viewpoint (cloud-top features and lightning). Data from different sources (reanalysis, satellite, radar, and pluviometers) were used in this study, and different methods were applied. The National Center for Monitoring and Early Warning of Natural Disasters (CEMADEN) registered accumulated rainfall above 400 mm between 26 April and 5 May using 27 pluviometers located in the central-northern part of RS. The monthly volumes reached 667 mm and 803 mm, respectively, for April and May 2024, against a climatological average of 151 mm and 137 mm for these months. The maximum precipitation recorded was 300 mm in a single day on 30 April 2024. From a large-scale point of view, an anomalous heat source in the western Indian Ocean triggered a Rossby wave that contributed to a barotropic anticyclonic anomalous circulation over mid-southeastern Brazil. While the precipitant systems were inhibited over this region (the synoptic view), the anomalous stronger subtropical jet southward of the anticyclonic circulation caused uplift over RS State and, consequently, conditions leading to mesoscale convective system (MCS) development. In addition, the low-level jet east of the Andes transported warm and moist air to southern Brazil, which also interacted with two cold fronts that reached RS during the 10-day period, helping to establish the precipitation. Severe deep MCSs (with a cloud-top temperature lower than $-80\text{ }^{\circ}\text{C}$) were responsible for a high lightning rate (above 10 flashes km^{-2} in 10 days) and accumulated precipitation (above 600 mm in 10 days), as observed by satellite measurements. This high volume of rainfall caused an increase in soil moisture, which exceeded a volume fraction of 0.55, making water infiltration into the soil difficult and, consequently, favoring flood occurrence.

Keywords: extreme precipitation; severe deep MCSs; floods; southern Brazil; teleconnection



Citation: Reboita, M.S.; Mattos, E.V.; Capucin, B.C.; Souza, D.O.d.; Ferreira, G.W.d.S. A Multi-Scale Analysis of the Extreme Precipitation in Southern Brazil in April/May 2024. *Atmosphere* **2024**, *15*, 1123. <https://doi.org/10.3390/atmos15091123>

Academic Editor: Mario Marcello Miglietta

Received: 2 August 2024

Revised: 4 September 2024

Accepted: 14 September 2024

Published: 16 September 2024



Copyright: © 2024 by the authors. Licensee MDPI, Basel, Switzerland. This article is an open access article distributed under the terms and conditions of the Creative Commons Attribution (CC BY) license (<https://creativecommons.org/licenses/by/4.0/>).

1. Introduction

Studies focusing on Brazil have shown that extreme daily precipitation events are becoming more frequent, particularly in the country's southern region [1,2]. Many of the reported episodes in the Brazilian literature are associated with high volumes of rainfall in less than 24 h. Due to this fact, the studies focus on describing the atmospheric systems that

cause extreme precipitation without investigating the large-scale background associated with them.

Some episodes of daily extreme rainfall resulted from mesoscale convective systems (MCSs) embedded in a cold front environment, such as the event in northern Rio Grande do Sul (RS) and Santa Catarina in June 2020 [3]. Convective rainfall and the influence of the South Atlantic Convergence Zone (SACZ) were responsible for heavy precipitation and, consequently, floods and landslides that devastated Petrópolis (Rio de Janeiro State) in 2022 [4–6]. The interaction of a cold front with topography has also caused significant precipitation on the north coast of São Paulo State, with the highest volume (683 mm in less than 15 h) ever recorded in Brazil [7]. Extratropical cyclogenesis over southern Brazil caused great damage in central-northern RS in 2023 [8,9]. Furthermore, subtropical MCSs, developing in response to upper- and low-level jets and two cold fronts, led to the highest volume of precipitation and floods in the climatological history of RS during ten days (from 26 April to 5 May) in 2024 (which is the focus of this study). Unlike the others mentioned, this anomalous episode shocked the world due to its drivers, persistence, and socio-environmental impacts [10].

Indeed, until 2024, the most severe precipitation event recorded in RS State was in May 1941, which raised the Guaíba River to a record height of 4.76 m on 8 May [11,12]. This record was surpassed by the accumulated rainfall from 26 April to 5 May 2024, which raised the Guaíba River to 5.35 m [12]. This heavy rainfall caused flooding in the regions that received precipitation and in remote areas along the Patos Lagoon. After 5 May, the rains continued in the central-northern and southern parts of RS, but the Guaíba River level did not exceed 5.35 m. From the end of April to 9 August 2024, the Civil Defense of RS reported that 478 municipalities were affected by both rain and flooding, representing 96% of the total municipalities, resulting in 183 deaths and 28 missing people, and a total of 2,398,255 people affected by the extreme event [13].

The increase in intensity and frequency of extreme precipitation events is a feature in Brazil and worldwide, as documented by annual reports such as the State of the Climate, a yearly publication of the American Meteorological Society. For instance, in 2023, the western and eastern parts of Africa were affected by extreme daily rainfall associated with different drivers [14,15]. Extreme events do not follow the same pattern in every region or part of the world. Each episode deserves special attention due to the multi-scale coupling that leads to different precipitation systems. Additionally, the resulting rainfall affects the area, with impacts exacerbated by the physical characteristics of the region, which was the case in the event in RS. Hence, these factors are the motivation for this study. Given this, the present study aims to carry out a multi-scale analysis of the extreme precipitation that occurred from 26 April to 5 May 2024 in RS State in Brazil. We describe the large-scale patterns that interacted with the South American synoptic environment and led to the MCS development. In addition, a more detailed analysis of the spatial pattern of cloud-top characteristics, precipitation, lightning, and soil moisture estimated from satellites and the vertical structure of precipitating clouds is presented. This study is organized as follows: Section 2 describes the study area, data, and methodologies applied, and Section 3 presents the results and discussions. It begins with the characterization of the precipitation and floods in RS, followed by an analysis of the dominant large-scale circulation and synoptic systems during the study period, and ends with a mesoscale overview of the case study. Finally, the main conclusions are presented in Section 4.

2. Materials and Methods

2.1. Study Area

The study area is RS, the most austral state in Brazil, which is located between the latitudes 27°05' S and 33°45' S and the longitudes 49°42' W and 57°40' W (Figure 1a). RS has diversified geography with five primary physiographic regions (Figure 1a): (a) the Uruguaio and Sul-Rio-Grandense highlands, which consist of elevated plateaus and hills ranging from 200 to 400 m; (b) the Periferic depression located inland from the coastal plain

between the Uruguai and Sul-Rio-Grandense and the Basaltic highlands, with altitude varying between 100 and 200 m, which is primarily an agricultural zone due to its fertile soils; (c) the Basaltic (Meridional) highlands located in the central-northern part of the state, with the highest altitude (regions of ~1400 m); (d) the Cuesta de Haedo located in the western portion of the state, with altitudes ranging from 300 to 800 m; and (e) the coastal plain extending along the Atlantic Ocean, consisting mainly of sandy beaches, dunes, lagoons, and wetlands, which is relatively flat and close to sea level [16].

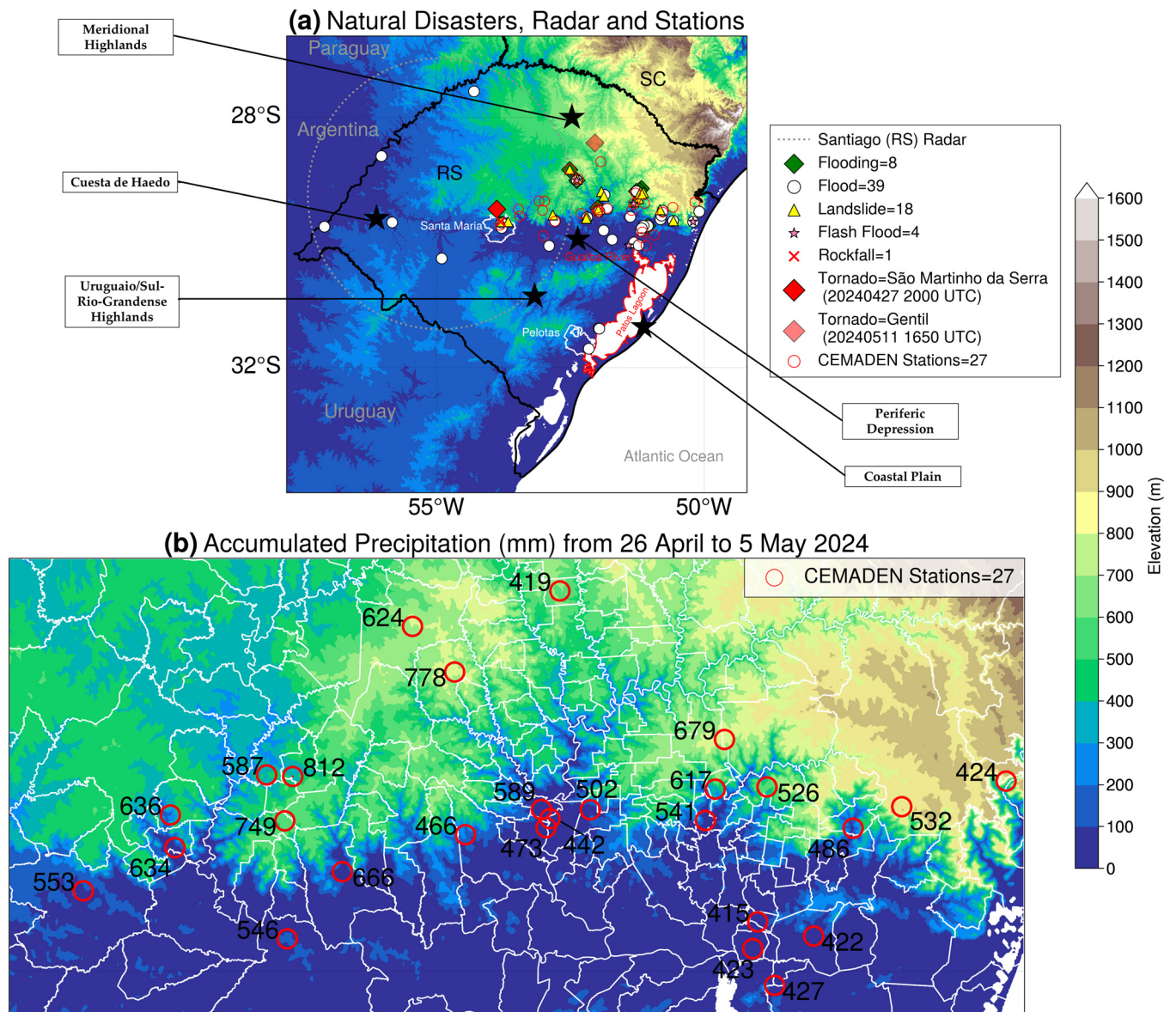


Figure 1. (a) Location of the Rio Grande do Sul (RS) and Santa Catarina (SC) States in Brazil (solid black line); Santiago weather radar (RS, dashed grey circle); natural disasters: flooding (green triangle), flood (white circle), landslide (yellow triangle), flash flood (pink star), rockfall (red cross), tornado (red diamond); and CEMADEN stations (open red circles). (b) Location of the National Center for Monitoring and Early Warning of Natural Disasters (CEMADEN) rain-gauge stations (open red circles) and accumulated precipitation (mm) from 26 April to 5 May 2024.

The region’s climate is subtropical, following the Köppen classification [17], with cold winters and warm summers. Its precipitation has a homogeneous distribution during the year [18], with a total precipitation of 1250 to 1650 mm in the southern part and 1450 to 1850 mm in the central-northern part of RS [19].

The rainfall from 26 April to 5 May 2024 caused this state’s worst flood in covered areas and water volume [11,12]. Figure 2 illustrates several problems caused by the rainfall and consequent floods. Figure 2 also shows images of tornadoes in the cities of São Martinho da Serra and Gentil (Figure 2e,f, respectively), whose locations are indicated in Figure 1a. One dramatic situation was the case of a horse (Figure 2d) named “Caramelo”, which stayed for more than 24 h on a house’s roof until it was rescued by firefighters [20].

2.2. Data

Data from different sources were used in this study, including disaster databases, records of severe weather, rain gauges, flooding mapping, grid-point datasets, climate indices, and satellite and radar estimates. The details of these datasets are provided as follows:

Disaster databases: Records of natural disasters from 26 April to 5 May 2024 provided by the National Center for Monitoring and Early Warning of Natural Disasters (CEMADEN) were used (Figure 1). The CEMADEN compiles information from the Civil Defense, National Center for Risk and Disaster Management (Cenad), reports from social media, and registers from its own analysis. This database provides the date, location, and typology of disasters, such as flooding, flood, landslide, flash flood, and rockfall. Records of severe weather from the Severe Weather Recording Platform (PRETS) [21] were used [22]. PRETS is part of a broader project called PREVOTS, which documents severe storm reports of hail, wind gusts, and tornadoes in Brazil. The reports are collected from several sources, including social media, news media, governmental institutions, and volunteer storm spotters. All reports are manually checked to ensure quality. This database provides the date, time, location, and type (hail, wind gusts, and tornadoes) of severe storms. For this study, only tornado records that were registered by photography were used.

Rain Gauges: Data from January to May 2024 collected from 27 pluviometers (Figure 1, Table 1) provided by the CEMADEN [23], located in or close to the disaster region and recording the highest rainfall volumes between 26 April and 5 May 2024, were used. The frequency of these data is 10 min. As the time series from the CEMADEN is not very long, we used data from the National Institute of Meteorology (INMET) [19] for climatological comparison. The INMET has only 13 meteorological stations in RS covering the climatological period (1991–2020). We selected the INMET stations closest to the CEMADEN station since only one station located in Santa Maria (29.727° S, 53.807° W) was chosen.

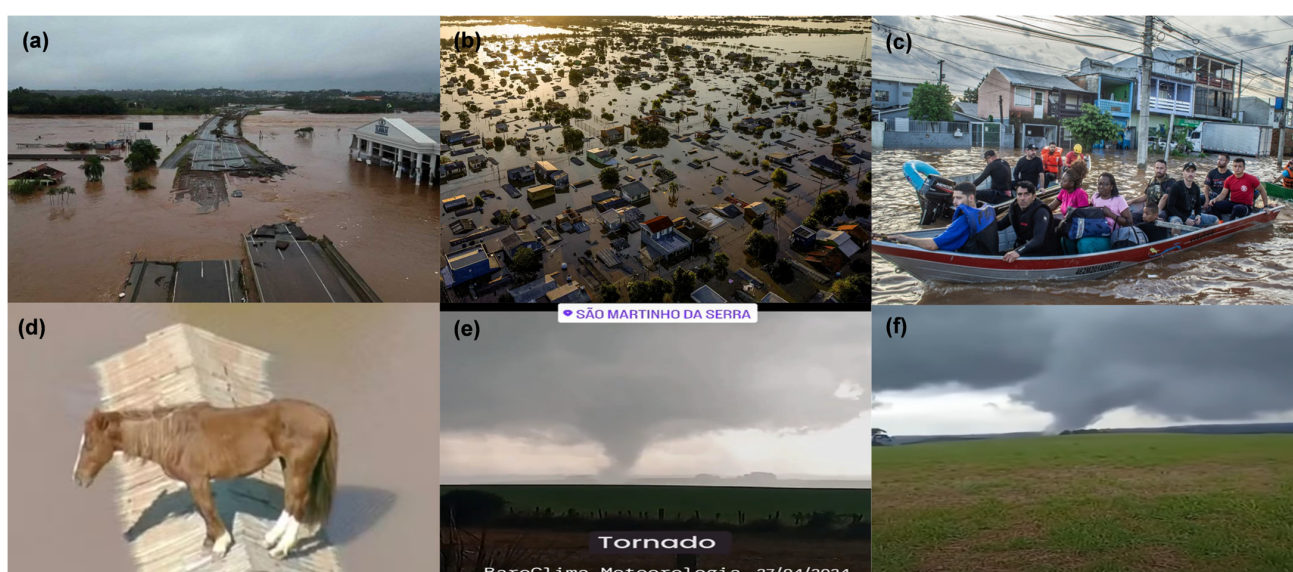


Figure 2. (a–f) Problems caused by the precipitation and floods in Rio Grande do Sul State from 26 April to 5 May 2024. Sources: (a) Correio Braziliense [24], (b) Agência Brasil [25], (c) Jovem Pan [26], (d) O Globo [27], (e) UOL [28], and (f) UOL [29].

Table 1. Information about the precipitation registered by the 27 rain-gauge stations from CE-MADEN: city, station name, latitude, longitude, and accumulated precipitation between 26 April and 5 May 2024.

Station Number	City	Station Name	Latitude	Longitude	Precipitation (mm)
1	Segredo	Prefeitura	−29.3399	−52.982	812.6
2	Fontoura Xavier	Centro	−28.9848	−52.3444	778
3	Lagoa Bonita do Sul	Centro	−29.49	−53.013	749.2
4	Caxias do Sul	Forqueta	−29.214	−51.282	679.6
5	Candelária	Fábrica de Injetados	−29.6629	−52.7873	666.8
6	Nova Palma	Centro	−29.47	−53.465	636.8
7	Faxinal do Soturno	Centro	−29.5809	−53.4467	634.8
8	Soledade	Centro	−28.8302	−52.5104	624.8
9	Alto Feliz	Alto Feliz	−29.382	−51.3176	617
10	Lajeado	Moinhos D'Água	−29.452	−52.003	589.4
11	Arroio do Tigre	Taboazinho	−29.3345	−53.0845	587.8
12	Santa Maria	Lorenzi	−29.727	−53.807	553.4
13	Cachoeira do Sul	Comunidade Três Vendas	−29.8908	−53.0043	546.4
14	Bom Princípio	Centro	−29.489	−51.356	541.2
15	São Francisco de Paula	Centro	−29.4417	−50.5828	532
16	Nova Petrópolis	Centro	−29.3756	−51.1144	526.2
17	Teutônia	Teutônia	−29.4524	−51.8097	502
18	Três Coroas	Rio Paranhana	−29.5157	−50.7742	486
19	Cruzeiro do Sul	Secretaria da Agricultura	−29.5132	−51.9848	473.2
20	Venâncio Aires	Centro Linha Brasil	−29.5371	−52.3016	466.8
21	Estrela	Indústrias	−29.4824	−51.9687	442.6
22	Viamão	Vila Augusta	−30.048	−51.084	427
23	Itati	Restaurante Mirador	−29.3549	−50.1719	424.93
24	Canoas	Marechal Rondon	−29.924	−51.17	423.4
25	Gravataí	Morungava	−29.8816	−50.93	422
26	Serafina Corrêa	Centro	−28.7102	−51.9298	419
27	Sapucaia do Sul	Paraíso	−29.833	−51.15	415

Flooding: The flood extent data were derived by Advanced Rapid Imaging and Analysis (ARIA) and Observational Products for End-Users from the Remote Sensing Analysis (OPERA) teams at NASA's Jet Propulsion Laboratory and the California Institute of Technology. The methodology used the Dynamic Surface Water Extent (DSW_x) products from OPERA, based on Harmonized Landsat Sentinel-2 (HLS) data. Specifically, two DSW_x-HLS images were used on 21 April 2024 and 6 May 2024. These images were reclassified into two new classes: (1) water and (2) not water. The difference between the two reclassified images was then calculated to identify areas of new water detection, interpreted as flood extent. The water class included DSW_x-HLS categories for open water, partial surface water, and HLS snow/ice, while the not water class included categories for non-water areas and HLS cloud/cloud shadow. From the Brazilian Institute of Geography and Statistics (IBGE), we obtained the Geospatial Database of street lines in Brazil that represents urban roads, urban expansions, and rural settlements across the country, including attributes such as street names, Census Sectors, and the National Address Database for Statistical

Purposes (CNEFE) for the year of 2022. It also provides estimates of the number of residences per location. Updated with each Demographic Census and continuously between censuses through high-resolution imagery and field campaigns, the database began with data from the 2007 Censuses, enhanced by vector data from municipal agreements and private companies. Essential for detailed geographic and statistical analyses, Street Faces supports political decision-making and public policy implementation, aiding the IBGE in planning, collecting, and disseminating census results and other surveys.

Grid-Point Datasets: ERA5 reanalysis from the European Centre for Medium-Range Weather Forecasts (ECMWF) [30] was used. Monthly averages from 1980 to 2023 for April and May were downloaded to compute climatologies, while hourly data (0000, 0600, 1200, and 1800 UTC) were obtained for the studied period (26 April–05 May 2024). Both periods were downloaded with a horizontal resolution of $0.25^\circ \times 0.25^\circ$. In addition, sea surface temperature (SST) anomalies from 1980 to 2023 were provided by the National Oceanic and Atmospheric Administration (NOAA OI SST V2 High-Resolution Dataset) [31]. This dataset has a daily frequency and horizontal resolution of $0.25^\circ \times 0.25^\circ$. Outgoing Longwave Radiation (OLR) was also obtained from the NOAA (CPC Daily Blended OLR) [32]. This dataset has a daily frequency and horizontal resolution of $2.5^\circ \times 2.5^\circ$.

Climate Indices: Monthly climate indices (Indian Ocean Dipole—IOD, Pacific Decadal Oscillation—PDO, El Niño-Southern Oscillation—ENSO, Niño 1 + 2, Niño 3, Niño 3.4, Niño 4, Atlantic Multidecadal Oscillation—AMO, Tropical North Atlantic Oscillation—TNA, and Tropical South Atlantic Oscillation—TSA) were obtained from the Teleconnection Online Tool [33,34].

Satellite Estimates: Brightness temperature, precipitation, lightning, and soil moisture data from satellite estimates were used. Brightness temperature was provided by the infrared channel (CH13, 10.35 μm) of the Advanced Baseline Imager (ABI) sensor on board the Geostationary Operational Environmental Satellite (GOES-16) satellite, which monitors the cloud-top characteristics [35]. The ABI sensor operates with a frequency of 10 min and has 16 channels [36]. This study used the CH13 infrared channel with 2 km of spatial resolution. Total lightning flash (intracloud and cloud-to-ground) from the Geostationary Lightning Mapper (GLM) on board the GOES-16 satellite was used. The GLM sensor captures radiance at the cloud-top at 777.4 nm to identify lightning during day and night [37], with efficiency exceeding 70%. The original data have 8 km and 20 s of spatial and temporal resolution, respectively, and are provided by the NOAA through Amazon AWS [38]. The data are accumulated in 5 min temporal intervals and provided by the Center for Weather Forecasting and Climate Studies and the National Institute for Space Research (CPTEC/INPE) [39]. Data from MERGE and Climate Hazards Center InfraRed Precipitation with Station data (CHIRPS) products were used for the precipitation spatial distribution analysis. MERGE is based on the precipitation provided by Global Precipitation Measuring (GPM) Integrated Multi-satellite Retrievals for GPM (IMERG) and combined with precipitation pluviometer measurements [40]. Data in hourly, daily, and monthly scales have been provided since 2000 by the CPTEC/INPE [41] with 10 km spatial resolution. CHIRPS is a quasi-global precipitation dataset combining precipitation data from satellite images and in situ station data [42]. The data have been available since 1981, with 0.05° and daily spatial and temporal resolution, respectively. The data were processed through Google Earth Engine [43]. Soil moisture from Soil Moisture Active Passive (SMAP) [44] was used. SMAP operates in polar orbiting with conical scanning and employs a microwave radiometer at 1.41 GHz and a Synthetic Aperture Radar (SAR) at 1.26 GHz. The data have 11 km and 3-hourly spatial and temporal resolution and were processed through Google Earth Engine [45]. Three SMAP products were used: top layer soil moisture (0–5 cm), root zone soil moisture (0–100 cm), and total profile soil moisture (0 to model bedrock depth).

Radar Estimates: The Constant Altitude Plan Position Indicator (CAPPI) of reflectivity from the Santiago weather radar was used. This radar is localized in RS State, installed at an altitude of 430 m, and operates in S-Band (2.7–2.9 GHz, 10.89 cm), with 15 elevations

(angles ranging from 0.4 to 18°) and a beam width of 2°. The radar is operated by the First Integrated Center of Air Defense and Air Traffic Control (CINDACTA I), belonging to the Department of Air Space Control (DECEA). It has a temporal resolution of 10 min. The CAPPI ranging from 2 to 15 km in height, with 1 km of vertical and horizontal resolution, was produced. Although other weather radars are available in RS, the Santiago Radar was the only one that captured the storms.

2.3. Analyses

The analyses described below were performed with the data in their original grid resolution, as presented in the previous section.

The extreme event: The extreme event of precipitation was initially characterized by an analysis of rainfall measured at the 27 rain gauge stations from the CEMADEN. In these stations, precipitation is accumulated in 10 min time intervals. For this work, we converted it on daily scale (from 0000 to 2359 UTC). The daily totals for the monthly scale were accumulated for January, February, March, April, and May 2024. The monthly precipitation of each CEMADEN station was compared with the climatology from the INMET. In addition, the time series of soil moisture from SMAP between April and May 2024 was obtained using the grid point closest to the location with the highest precipitation volume (Segredo City at 29.3399° S, 52.9820° W) determined within a 20 km buffer.

Flooding: The flooding area was defined using OPERA DSWx-HLS to identify surface water using the B01_WTR layer. The two images from 21 April 2024 and 6 May 2024 were examined for this analysis. Each image consisted of multiple Military Grid Reference System (MGRS) tiles, merged to create a composite image saved as a GeoTIFF file. The merging of these tiles ensured comprehensive spatial coverage of the area of interest. The reclassification and subsequent differencing of the images were crucial for accurately capturing the flood extent despite some challenges, such as misclassifying sediment-rich water as snow/ice in the HLS data. This methodology allowed for a precise delineation of flooded areas, aiding in assessing and responding to the flooding event.

Large-scale analysis: The primary purpose of this analysis is to describe the large-scale anomalies that can explain the circulation anomalies over Brazil during the study period. In other words, we investigated how large-scale circulation contributed to developing the synoptic systems that led to extreme precipitation. To achieve this, we present the anomalies for April 2024 for some variables (SST and OLR) and analyze others (stream function, velocity potential, and irrotational wind) by periods: the average of 1–30 April, 1–15 April, 16–30 April, and 26 April–5 May 2024. Anomalies were computed by taking the difference between 26 April and 5 May 2024 and the climatology from April to May (1980–2023). Notably, the stream function is a variable based on the rotational component of the wind, allowing for the analysis of cyclonic and anticyclonic action centers in the troposphere. This variable's negative (positive) values in the Southern Hemisphere are related to anomalous high (low) pressure centers. Velocity potential and irrotational wind help identify areas of large-scale ascending and descending movements. Velocity potential indicates large sources of wind divergence in the tropics, which are fundamental for generating Rossby waves. Negative (positive) values of velocity potential refer to anomalous uplift (subsidence) areas. Additionally, OLR indicates regions of tropical convection are favorable as a source of Rossby waves.

Synoptic scale analysis: The main purpose of this analysis is to describe the synoptic pattern favorable to cloud development and extreme precipitation over southern Brazil. To achieve this objective, we present wind anomalies at 200 and 850 hPa computed by subtracting the April–May climatology of 1980–2023 from the average of 26 April–5 May 2024. Mass divergence (D) was calculated in spherical coordinates, according to Equation (1):

$$D = \frac{\partial u}{a \cos \varphi \partial \lambda} + \frac{\partial v}{a \partial \varphi} \quad (1)$$

where u and v are, respectively, the zonal and meridional horizontal wind components, a is the Earth's radius, φ is the latitude, and λ is the longitude. The vertically integrated moisture flux divergence (*VIMF*) was calculated with Equation (2), following Peixoto and Oort [46]:

$$VIMF(\lambda, \varphi) = \int_0^{p_0} q \frac{dp}{g} \quad (2)$$

where q represents specific humidity, p is the pressure, g is the gravity acceleration, and p_0 the superior limit of integration. In this study, *VIMF* was calculated considering the levels between 1000 and 200 hPa. Additionally, we computed the divergence of *VIMF* by using its components (Q_λ and Q_φ) in the expression of mass divergence (D).

$$Q_\lambda = \int_0^{p_0} qu \frac{dp}{g} \quad (3)$$

$$Q_\varphi = \int_0^{p_0} qv \frac{dp}{g} \quad (4)$$

Mesoscale and cloud features analyses: The main goal of this analysis is to describe the cloud and precipitation features from satellite and radar images. Daily precipitation from MERGE and CHIRPS between 26 April and 5 May 2024 was used to represent the spatial distribution of precipitation in RS State. Cloud-top temperature (in this study obtained from the CH13 GOES-16 satellite) is related to cloud depth and is a proxy for strong convection [6,47,48]. Typically, deep clouds have higher graupel, ice crystals, supercooled water volume, and stronger updrafts, which are conditions favorable to lightning formation [49,50]. For that reason, lightning spatial distribution was analyzed. The total lightning from GOES-16 with a 5 min temporal scale was accumulated between 26 April and 5 May 2024. In addition, the spatial distribution of maximum soil moisture at the surface (top layer soil moisture between 0 and 5 cm in volume fraction units) between 26 April and 5 May 2024 was determined. The CAPPI sequential images of reflectivity from the Santiago radar were constructed to describe the precipitation structure of storms. In order to evaluate the vertical structure of some storms, vertical cross-sections of reflectivity were generated for the times closest to when the tornado registered at São Marinho da Serra City.

3. Results and Discussion

3.1. Precipitation and Flood

The monthly climatological distribution of precipitation in RS between January and May (INMET climatology, 1991–2020) is quite homogeneous, with totals not exceeding 200 mm/month (Figure 3a, blue bars). However, in 2024, from January to May, records from 27 rain gauges distributed across the state's central-northern region (Figure 1b and Table 1) indicated an increase of more than four times the climatology for April and May (Figure 3a). For example, the maximum monthly precipitation registered by rain gauges was 667 and 803 mm in April and May, respectively, while the climatology was 151 mm and 137 mm/month, respectively. These results are consistent with the meteorological stations from the INMET, which registered 617.1 mm for Santa Maria City during May 2024, while the climatological mean was 136.6 mm [19,51].

Between 26 April and 5 May 2024 (Figure 1b and Table 1), the accumulated precipitation ranged from 415 to 812.6 mm. On a daily scale, April 30th was the day with the highest accumulation between April 1st and May 31st, with values exceeding 300 mm in 24 h (Figure 3b). Both daily and monthly accumulated precipitation in 2024 is unusually high compared with recent disasters registered in Brazil. For example, Baixada Santista on 2nd–3rd March 2020 (700–880 mm month⁻¹ and 175–300 mm day⁻¹) [48], Petrópolis in February 2022 (620 mm month⁻¹ and 250 mm day⁻¹) [6], and the Metropolitan Re-

gion of Belo Horizonte in January 2020 (240 mm day^{-1}). Consequently, soil moisture presented a systematic increase from the beginning of April, reaching maximum values of approximately 0.55 (volume fraction, Figure 3c) close to 6 May 2024.

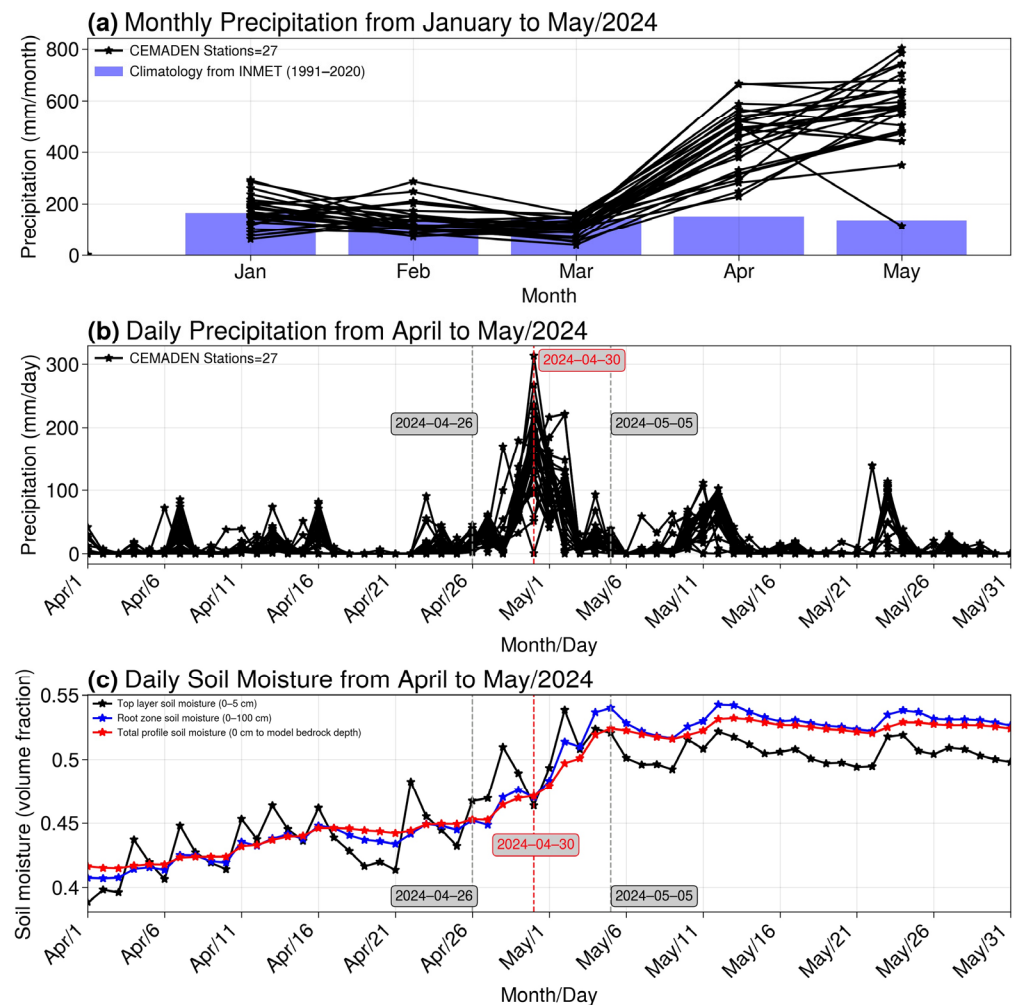


Figure 3. (a) Monthly precipitation recorded by 27 CEMADEN stations (black line) from January to May 2024 and precipitation climatology from INMET for the 1991–2020 period. (b) Daily precipitation from April to May 2024 was recorded by 27 CEMADEN stations (black line). (c) Daily moisture from April to May 2024 from SMAP for top layer soil moisture (0–5 cm, black line), root zone soil moisture (0–100 cm, blue line), and total profile soil moisture (0 to model bedrock depth, red line). Figures (a) and (b) indicate the period with the heaviest precipitation with grey and red boxes.

We used the disaster database from the CEMADEN to quantify the problems in the central-northern area of RS (Figure 1a). Note that the CEMADEN monitors only a limited number of municipalities in each Brazilian state, so the numbers presented here refer only to the monitored areas. A total of 70 disasters occurred between 26 April and 5 May 2024, with the majority being flood (56%), followed by landslide (26%) and flooding (11%) (Figure 1a). These disasters occurred in the area with the highest precipitation volume registered by the CEMADEN's stations (Figure 1b). Most disasters occurred along the edges of regions with steep topography, particularly landslides, flooding, and rockfalls. In addition, several floods (white circles) occurred near rivers, as observed on the west side of the map and close to the Patos Lagoon (Figure 1a).

Here, we provide a more detailed analysis of the flood events in RS using satellite-derived flood extent data and residential information from the IBGE. The flood extent map highlights the areas affected by flooding (Figure 4). The Metropolitan Region of

Porto Alegre (RMPOA) experienced the highest impact. Figure 5 provides a zoomed-in view of the metropolitan region, emphasizing the severity of the flooding in this densely populated area.

By overlaying the satellite-derived flood extent map with the residential data provided by the IBGE, we could calculate the number of houses affected by the flood in each mesoregion of RS. This method provided a comprehensive overview of the flood’s impact on residential areas, enabling a targeted response to the affected regions. In the RMPOA, the most urbanized and densely populated state, 335,552 residences were affected by flood (Figure 5). This massive number of affected residences highlights the critical importance of urban flood management and the necessity for robust infrastructure to mitigate future flood risks.

Other mesoregions also experienced varying degrees of impact. The Southeast Region had 49,865 affected residences, followed closely by the Central-East Region with 48,293 impacted homes. The Central Region had 1376 affected residences, the Northeast Region had 1519, the Northwest Region had 5185, and the Southwest Region had 3813. These numbers illustrate the widespread flooding across the state and each region’s diverse challenges. The comprehensive evaluation provided by this analysis is crucial for guiding disaster response and recovery efforts, ensuring that resources are allocated efficiently to the areas most in need.

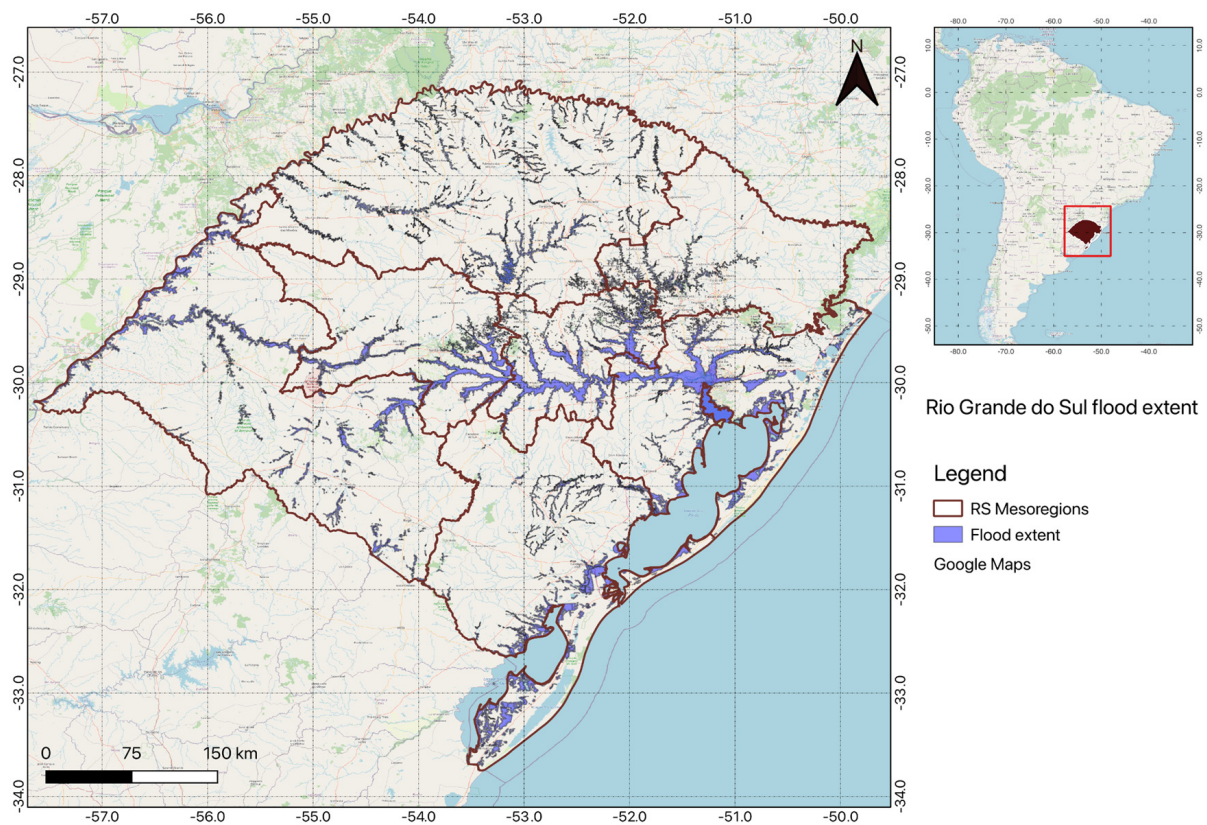


Figure 4. Flooding area (dark blue) of ARIA/OPERA derived from DSWx-HLS and political mesoregions of Rio Grande do Sul State. In the upper-right figure, the red square highlights the RS state, that has been zoomed in and displayed in the left figure.

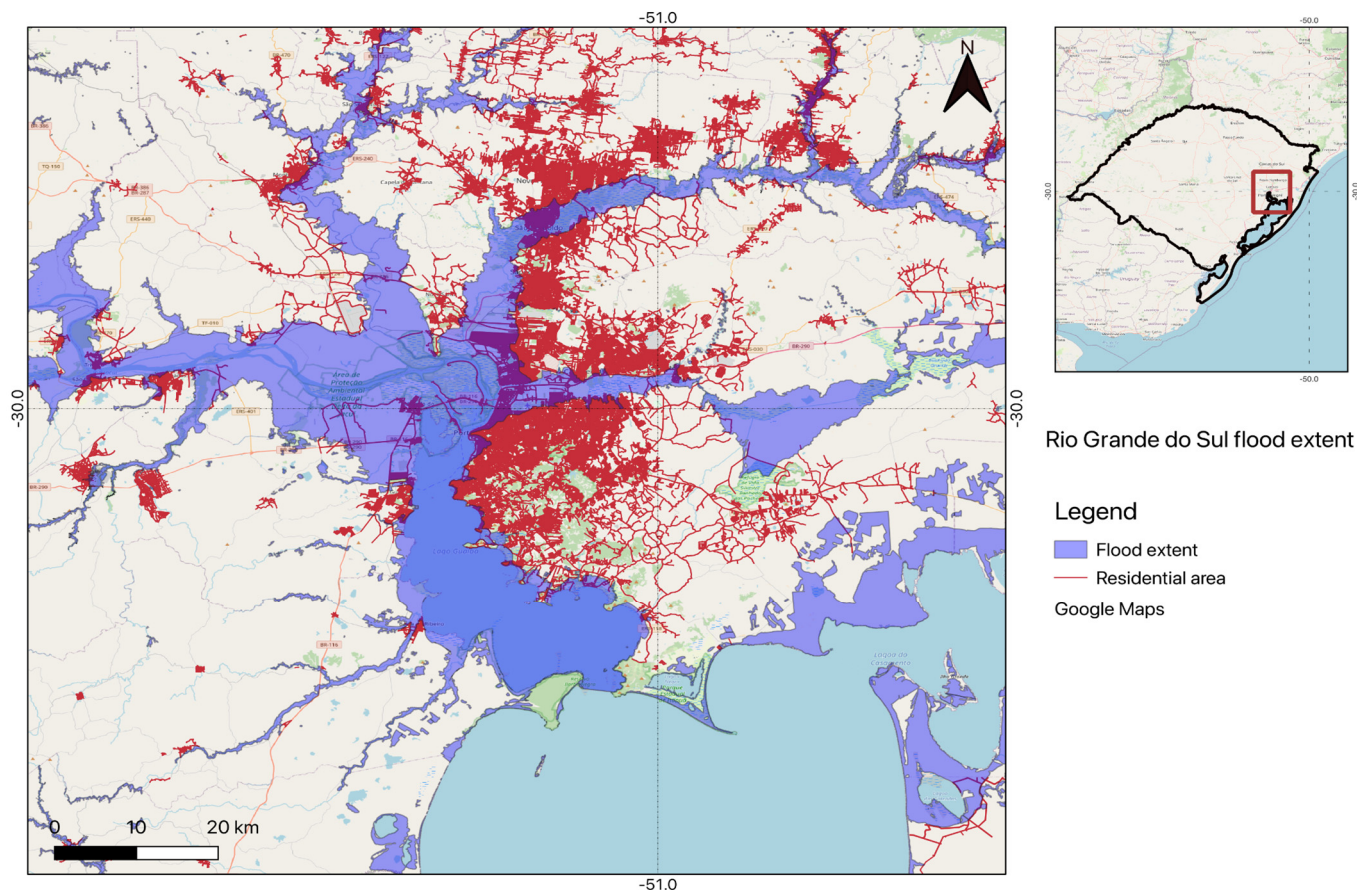


Figure 5. Flooding area (dark blue) of ARIA/OPERA derived from DSWx-HLS over the metropolitan region of Porto Alegre and the residential areas. Number of houses impacted by flood is in RMPOA: 335.552, Southeast: 49.865, Central-East: 48.293, Central: 1376, Northeast: 1.519, Northwest: 5.185, and Southwest: 3.813. Residential areas are indicated in red on the map. In the upper-right figure, the red square highlights the area that has been zoomed in and displayed in the left figure.

3.2. Large-Scale Circulation

Figure 6 presents the SST anomalies for April, along with the indices of the major oceanic oscillations: IOD, PDO, ENSO, AMO, TNA, and TSA. Unprecedented high temperatures in the Atlantic Ocean basin's northern and southern tropical sectors were recorded in April 2024 [34]. In the North Atlantic, positive TNA is associated with the extremely positive phase of AMO. Regarding the Pacific Ocean, the warm phase (El Niño) of the ENSO phenomenon was in the process of weakening during April (with Niño 3.4 region/ONI = 0.98 °C; the time evolution of this index can be seen in [52]). Although anomalously cold waters prevailed in the Niño 1 + 2 region (Figure 6), the index was still positive (0.32 °C), as in the other ENSO areas. In the Indian Ocean, April was characterized by neutral conditions (IOD = 0.31 °C) since the dipole index was lower than one standard deviation, as Reboita et al. [53] suggested. However, anomalous warming occurred throughout the Indian Ocean basin, especially in the tropical sector along the coast of Somalia. Hence, it is proposed that the coupling of El Niño and the warming of the Indian Ocean basin may have contributed to the extreme precipitation in southern Brazil, as previously highlighted by Taschetto and Ambrizzi [54] and discussed in this section.

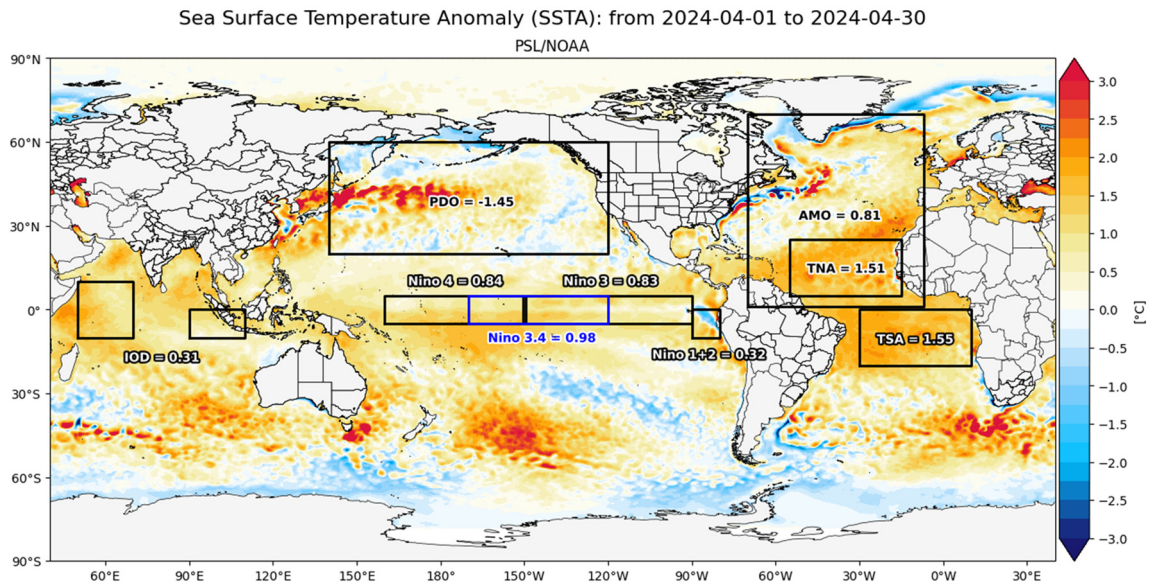


Figure 6. April 2024 climate indices and global SST anomalies ($^{\circ}\text{C}$) based on the OISSTv2 dataset.

The SST anomalies in Figure 6 are heat sources contributing to the atmosphere’s convective processes. A proxy variable for identifying areas of intense convection is OLR. Low values of OLR (and negative anomalies) indicate a lower amount of infrared radiation leaving the atmosphere, which occurs in cloud-covered regions. In the global analysis (Figure 7), the western Indian Ocean stands out as the area of highest convective activity in the tropics (lowest OLR value). However, negative OLR anomalies also appear in the Tropical Atlantic and north of Australia. In the subtropics, the region with negative OLR anomalies in southern Brazil is particularly notable (Figure 7).

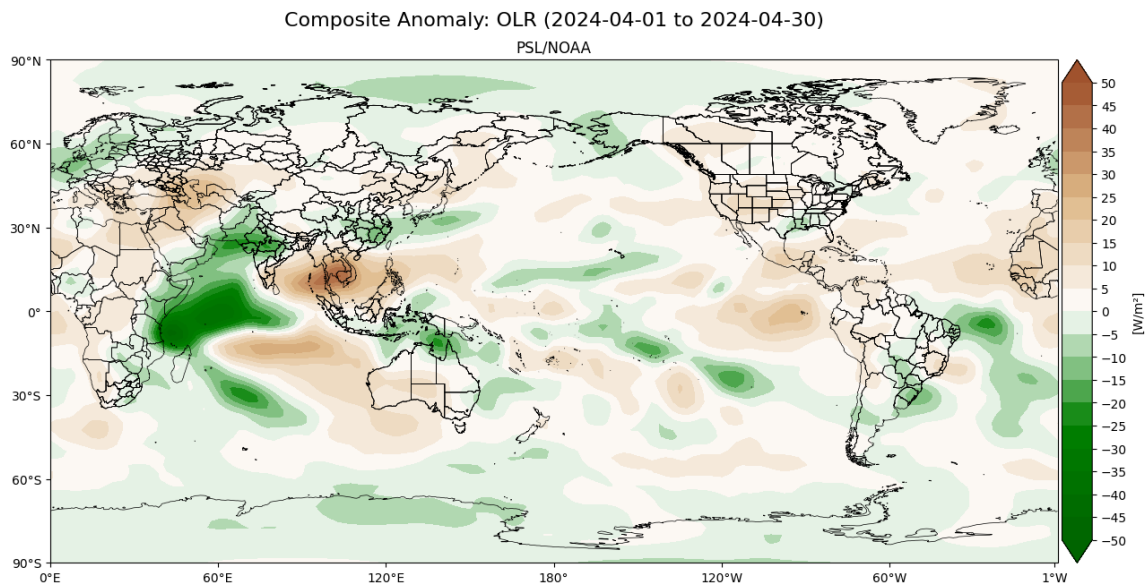


Figure 7. April 2024 OLR anomalies (W m^{-2}) based on NOAA dataset.

Due to the intense signal of negative OLR anomalies in the Indian Ocean, Figure 8a provides a zoomed-in view of this ocean basin. The negative OLR anomalies extend from the eastern coast of Africa to central portions of the Indian Ocean. They also spread to the north, covering southern Arabia and reaching as far as India. In a joint analysis with the SST (Figure 8b), there is a vast region of intense warming in the Indian Ocean, especially along the coast of Somalia, where positive SST anomalies exceed 2°C ($\text{SST} > 30^{\circ}\text{C}$). Most of the

oceanic area north of Madagascar recorded values above $1.5\text{ }^{\circ}\text{C}$ in April 2024. This condition in the Indian Ocean contributed to the historic floods recorded in East African countries, leading to the deaths of 473 people and affecting about 1.6 million individuals [55]. Somalia, Tanzania, Ethiopia, Kenya, Uganda, and Burundi were the most impacted countries.

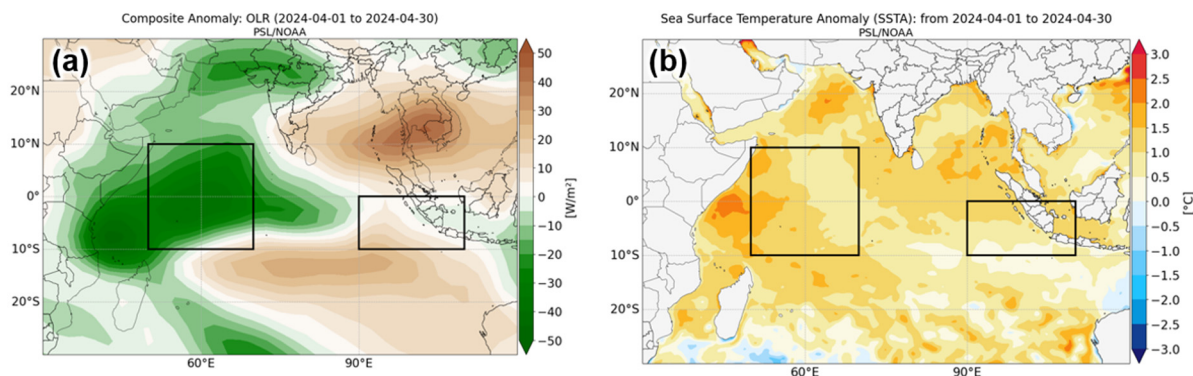


Figure 8. Zoomed-in view of the April 2024 anomalies in the Indian Ocean: (a) OLR anomalies (W m^{-2}) and (b) SST anomalies ($^{\circ}\text{C}$). The black boxes indicate the areas used to compute IOD.

Since warm ocean waters are not always associated with anomalous convection in the tropics, the joint analysis of OLR anomalies and tropical disturbances using a Hovmöller diagram (Figure 9) can indicate potential storm-triggering mechanisms. Around 60° E longitude, negative OLR anomalies predominated throughout April 2024 (Figure 9), with simultaneous occurrences of low-frequency variability (purple contour) and Kelvin waves (blue contour). At the end of April, an even more constructive interaction of tropical variability modes occurred, with the Madden–Julian Oscillation (MJO) overlapping the other signals (Figure 9). Thus, the interaction between tropical variability modes and the warm waters in the western Indian Ocean was the main driver of deep convection in this part of the tropics.

Since the Indian Ocean was an important source of anomalous heat for the tropical atmosphere, which responded with a large and intense area of convection, this condition may have contributed to the dispersion of large-scale waves (acting as teleconnection patterns) that could explain the extreme precipitation in southern Brazil. The atmospheric circulation was analyzed through velocity potential anomalies and stream function at 250 hPa in different periods (Figure 10) to investigate this feature.

In April 2024 (Figure 10a), the velocity potential anomaly shows ascending movements in the western Indian Ocean in response to intense convection (Figures 8 and 9). An individual analysis of April's first and second halves (Figure 10c,f) highlights that the anomalous convection north of Madagascar was more intense in the first half (Figure 10c). A teleconnection pattern gradually formed between the Madagascar region and the South Pacific Ocean through interspersed action centers (Figure 10d).

During the second half of April, the storms remained concentrated in the western Indian Ocean (Figure 10e). During this period, the complete propagation of Rossby waves was established between the South Pacific and South America (Figure 10f). There was a strong amplification of the waves, characterized by a large amplitude ridge at 120° W , a downstream trough in Patagonia, and a ridge over south-central Brazil. The ridge over Brazil and the South Atlantic Subtropical Anticyclone (SASA) intensified this (more details on regional impacts are presented in the next section). The amplification of planetary waves from the South Pacific toward the South American continent is mainly attributed to the conservation of absolute vorticity due to latitude variations along the wave trajectory and constructive interaction, i.e., the superposition of waves. Between late April and early May (the period of the greatest impact of rains and floods in RS), the large-scale pattern maintained almost the same signal observed in the second half of April but with greater intensity. Finally, we can infer that the substantial wind divergence in the Western Pacific

throughout April (Figure 10a) played a fundamental role in the teleconnection process observed this month, as evidenced by the wave train in Figure 10b.

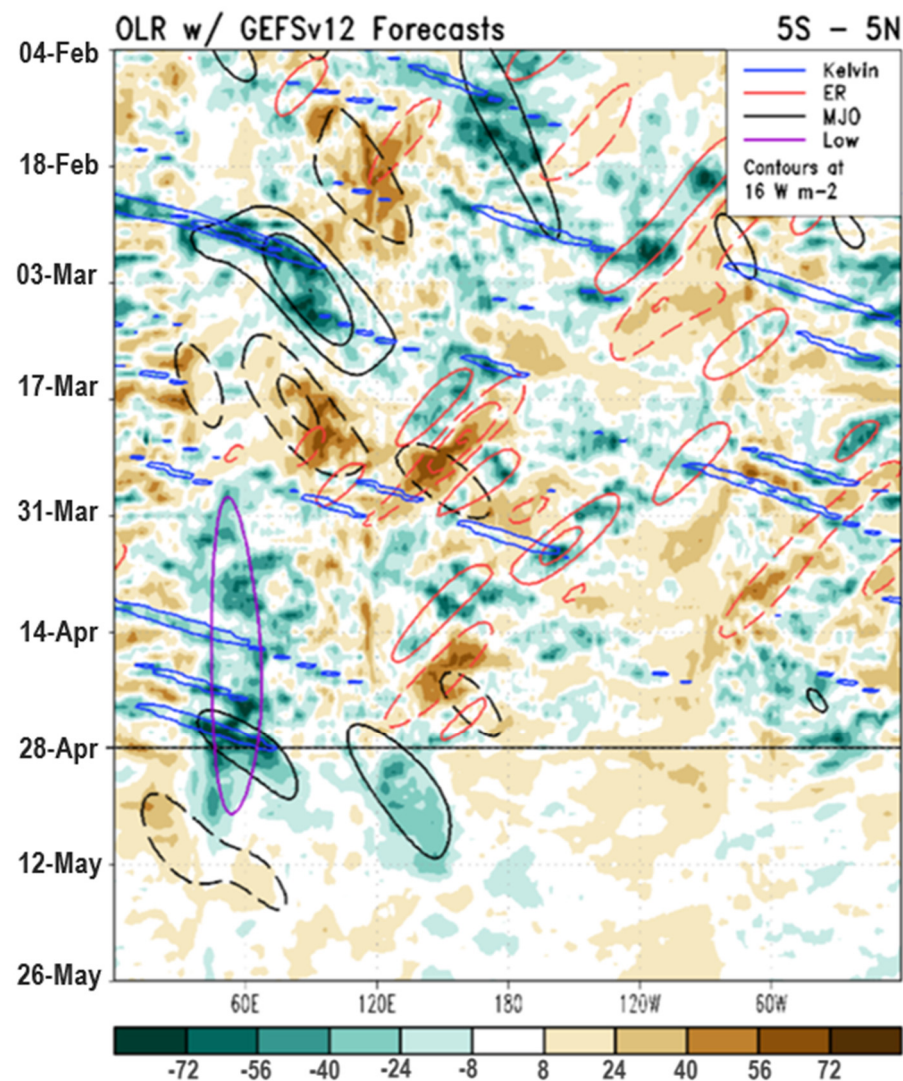


Figure 9. Hovmöller diagram for OLR anomalies (shaded change at $16 W m^{-2}$) averaged between $5^{\circ} N$ and $5^{\circ} S$ and tropical disturbances (in colored lines). The x-axis represents longitudes, and the y-axis represents time. Source: NOAA [56].

Figure 11 illustrates the dynamic of the Rossby wave dispersion in April 2024 over the Southern Hemisphere. The combination of the variables of the velocity potential anomaly, irrotational wind anomaly, and stream function anomaly indicates that the strong upper-level wind divergence associated with ascending movements in the western Indian Ocean was the necessary condition for the emergence of two Rossby waves adjacent to the maximum source of anomalous heat in the tropics. This observed pattern is consistent with the conceptual model proposed by Rossby and described by Karoly [57] and Trenberth et al. [58].

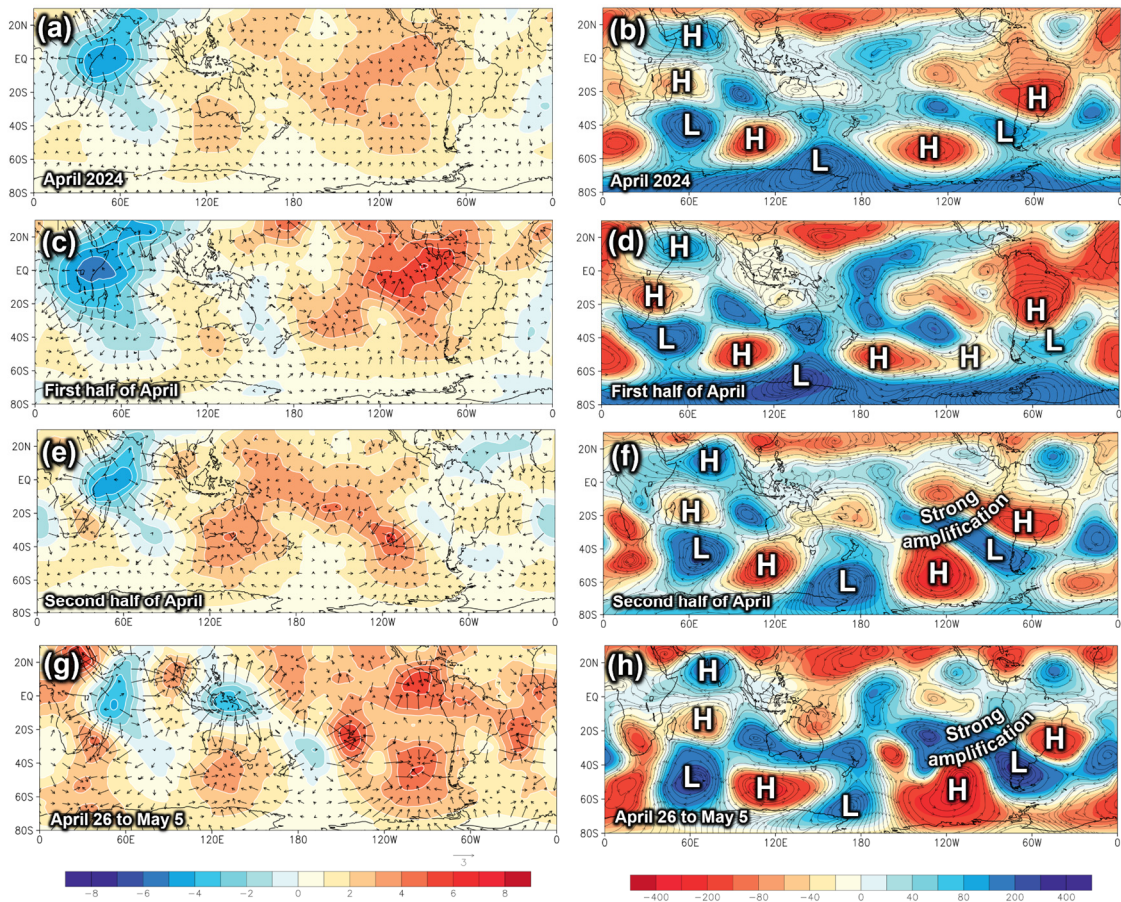


Figure 10. (a,c,e,g) Velocity potential anomaly ($10^6 \text{ m}^2 \text{ s}^{-1}$) (shaded) and divergent wind component (m s^{-1} ; arrows) at 250 hPa (right panel) and (b,d,f,h) stream function anomaly ($10^6 \text{ m}^2 \text{ s}^{-1}$) at 250 hPa. Letters L and H indicate low- and high-pressure anomalous centers, respectively.

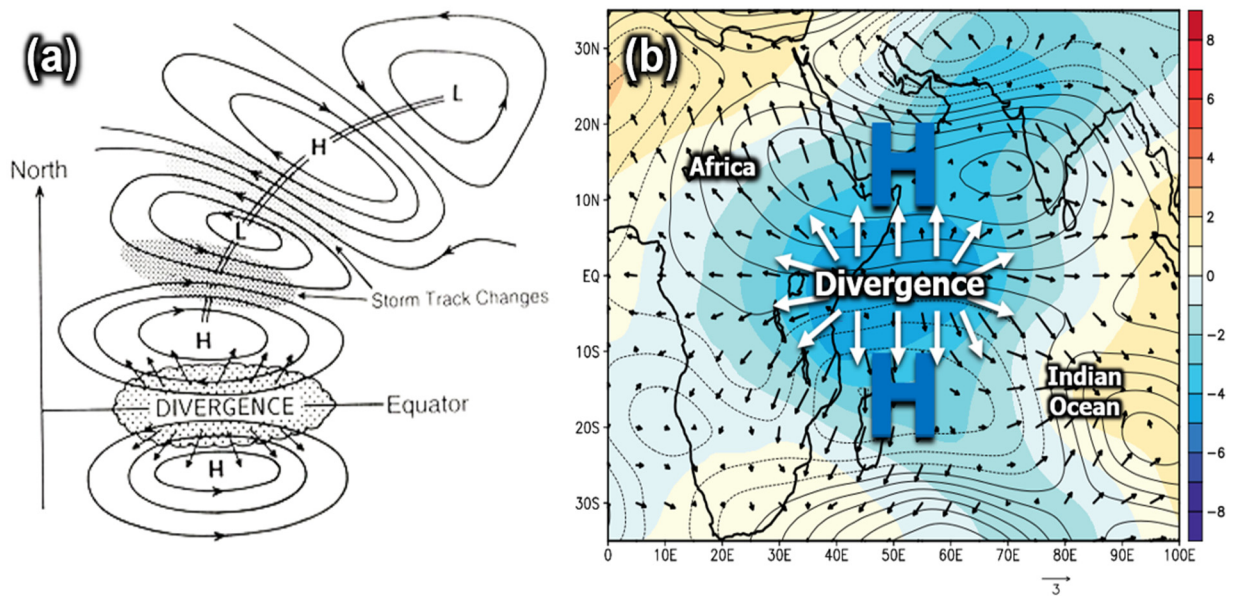


Figure 11. Comparison between (a) a conceptual model of the Rossby wave dispersion at upper levels associated with tropical convection [58] and (b) the case of April 2024: 250 hPa stream function anomaly ($10^6 \text{ m}^2 \text{ s}^{-1}$; contour), velocity potential anomaly ($10^6 \text{ m}^2 \text{ s}^{-1}$; shaded), and divergent wind component (m s^{-1} ; arrows). Letter H indicates high-pressure anomalous centers.

3.3. Synoptic Scale

The global-scale patterns discussed in Section 3.2 are associated with the synoptic scale configuration in South America to explain the extreme precipitation event between 26 April and 5 May in southern Brazil. Figure 10d shows that the wave train originating from the Indian Ocean exhibits strong amplification between the Pacific Ocean and South America. This large-scale anomalous pattern explains the presence of the anomalous cyclonic circulation center at 250 hPa over Patagonia and the anticyclonic center over parts of central, southeastern, and southern Brazil (Figure 12a). These two circulation systems, located at the end of the Rossby wave trajectory in the Southern Hemisphere, contribute to intensifying the subtropical jet, which shows a strength of about 30 m s^{-1} above average over the La Plata river discharge (Figure 12a). This anomalous signal in the upper-level wind field reveals that from 26 April and 5 May, positively oriented troughs (the northwest-southeast axis) occurred in the south of the continent, and a more intense jet stream flow downstream accompanied the southern sector of the strong ridge positioned over parts of Brazil.

The barotropic nature of Rossby waves [59–61] becomes evident when the anomalous circulation fields at 250 and 850 hPa are compared (Figure 12), as the locations of these centers are similar at both levels. The anticyclonic action center at 250 hPa, when coupled with the SASA [62], intensifies it throughout all tropospheric layers. This change in high- and low-level atmospheric circulation during the event impacted the central-southeastern and southern regions of the country differently. While the high-pressure system over much of Brazil inhibited ascending movements in the atmosphere and cloud development, its contribution to accelerating the subtropical jet over RS led to regions of mass divergence in this location (Figure 12a) and, consequently, to the development of deep cloud clusters in the atmosphere (Figure 13). Divergence in the upper levels of the atmosphere is a dynamic mechanism of airlifting, and removing air from the atmospheric column contributes to the reduction of near-surface pressure. In the case of RS, the air rising in the atmosphere was warm and humid, thus providing suitable conditions for cloud formation.

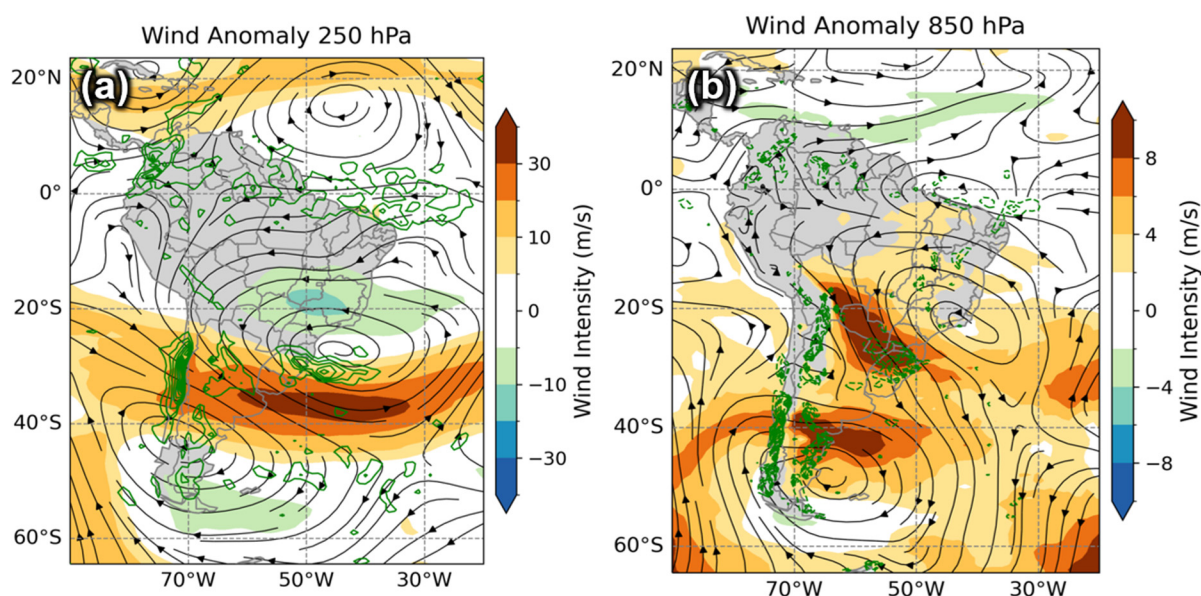


Figure 12. Anomaly of wind magnitude (m s^{-1} , shaded) and streamlines at (a) 250 hPa and (b) 850 hPa. The anomaly is obtained by the difference between the average from 26 April and 5 May and the average for April and May from 1980 to 2023. Green continuous lines indicate (a) divergence higher than $0.5 \times 10^{-5} \text{ s}^{-1}$ and (b) convergence lower than $-0.3 \times 10^{-5} \text{ s}^{-1}$, both for the event average.

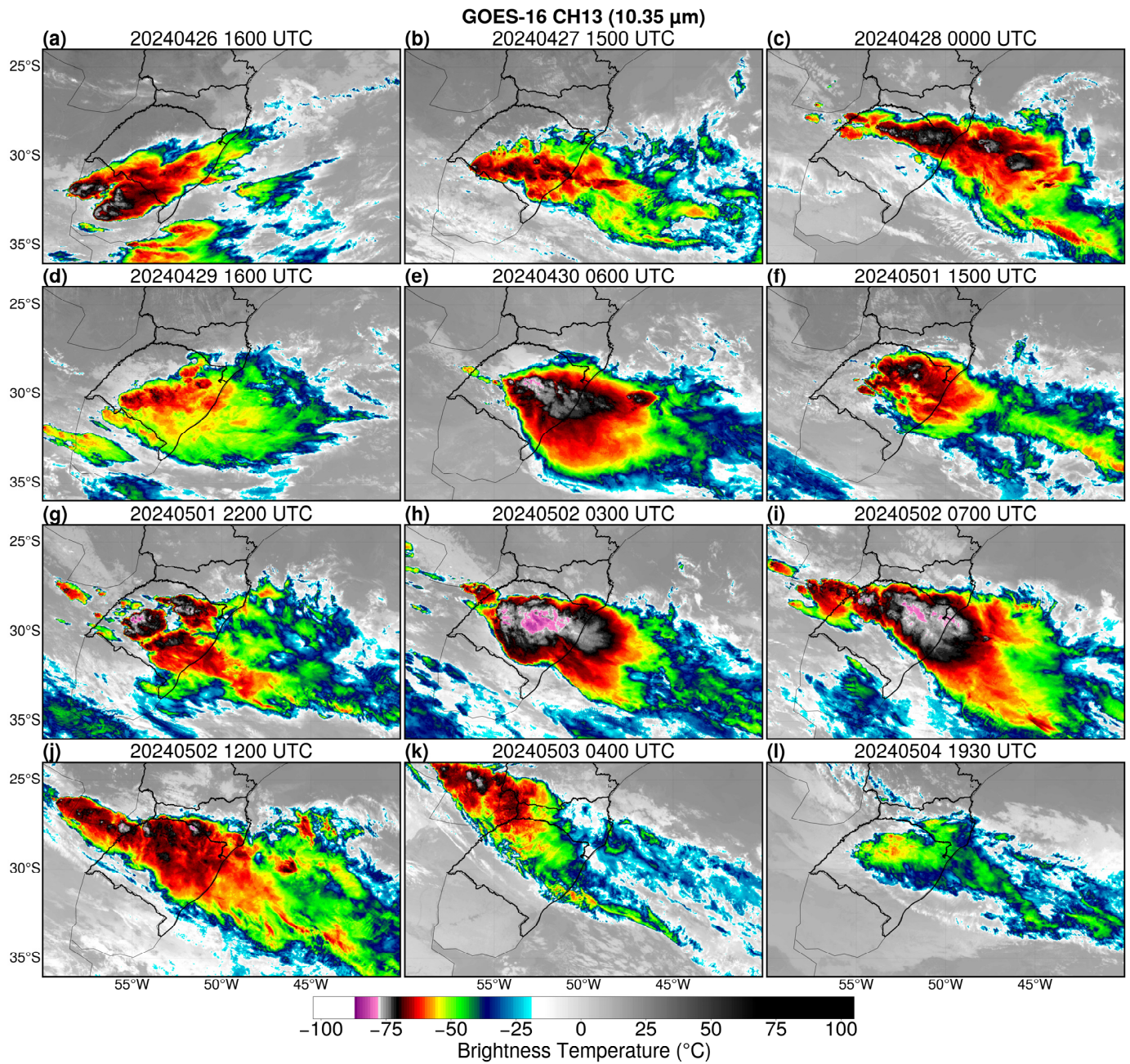


Figure 13. (a–l) Brightness temperature (°C) images from the infrared channel (CH13, 10.35 μm) provided by the ABI sensor aboard the GOES-16 satellite from 26 April 2024 at 1600 UTC to 4 May 2024 at 1930 UTC.

With the intensified subtropical gyre of the SASA at 850 hPa, the low-level jet east of the Andes (LLJ) gains strength from northern Bolivia to southern Brazil. This pattern results in strong wind convergence at the exit of the LLJ at 850 hPa and divergence at 250 hPa at the latitudes of RS (Figure 12b), which is another indication of the coupling between low and high levels of the atmosphere. The combination of the ascending movements due to mass divergence provided by the subtropical jet over RS and the transport of warm and humid air by the LLJ (Figure 12) was the necessary “ingredients” for the development of MCSs (Figure 13) in the subtropics of South America, which follow the conceptual model presented in Silva Dias [63] and Martinez and Solman [64]. Therefore, most of the rainfall during the extreme event in the country’s south was associated with these systems. On the other hand, the anomalous cyclonic gyre in the south of the continent at 850 hPa was crucial

for generating cold air pulses that brought frontal systems to meet the LLJ in southern Brazil. The low-pressure area associated with the passage of a cold front on 27 April was also crucial for channeling the LLJ toward southern Brazil and establishing the first heavy rains in RS. This cold front reached the extreme south of Brazil at 1200 UTC on 27 April, moved northeast, reaching the central-northern part of RS at 0000 UTC on 28 April, and migrated to the Atlantic Ocean in the following hours. In total, two cold fronts passed through RS during the study period. The second system approached the extreme south of the country at 1200 UTC on 1 May and, after 24 h, was located in the northern part of the state (figures not shown).

Oceanic variables and the integrated tropospheric moisture flux divergence were analyzed to investigate the origin of the moisture responsible for the heavy rains that hit the southern region (Figure 14). From an oceanic perspective, Figure 14a shows the SST anomaly and the average of this variable during the extreme event (26 April and 5 May). The Tropical Atlantic presented record warming during the first half of 2024, which persisted from April to May. Temperatures close to 30 °C (Figure 14b), associated with widespread positive anomalies, were observed along the entire northern coast of Brazil. This condition of the Atlantic Ocean resulted in greater evaporation, increasing the amount of water vapor available in the lower troposphere.

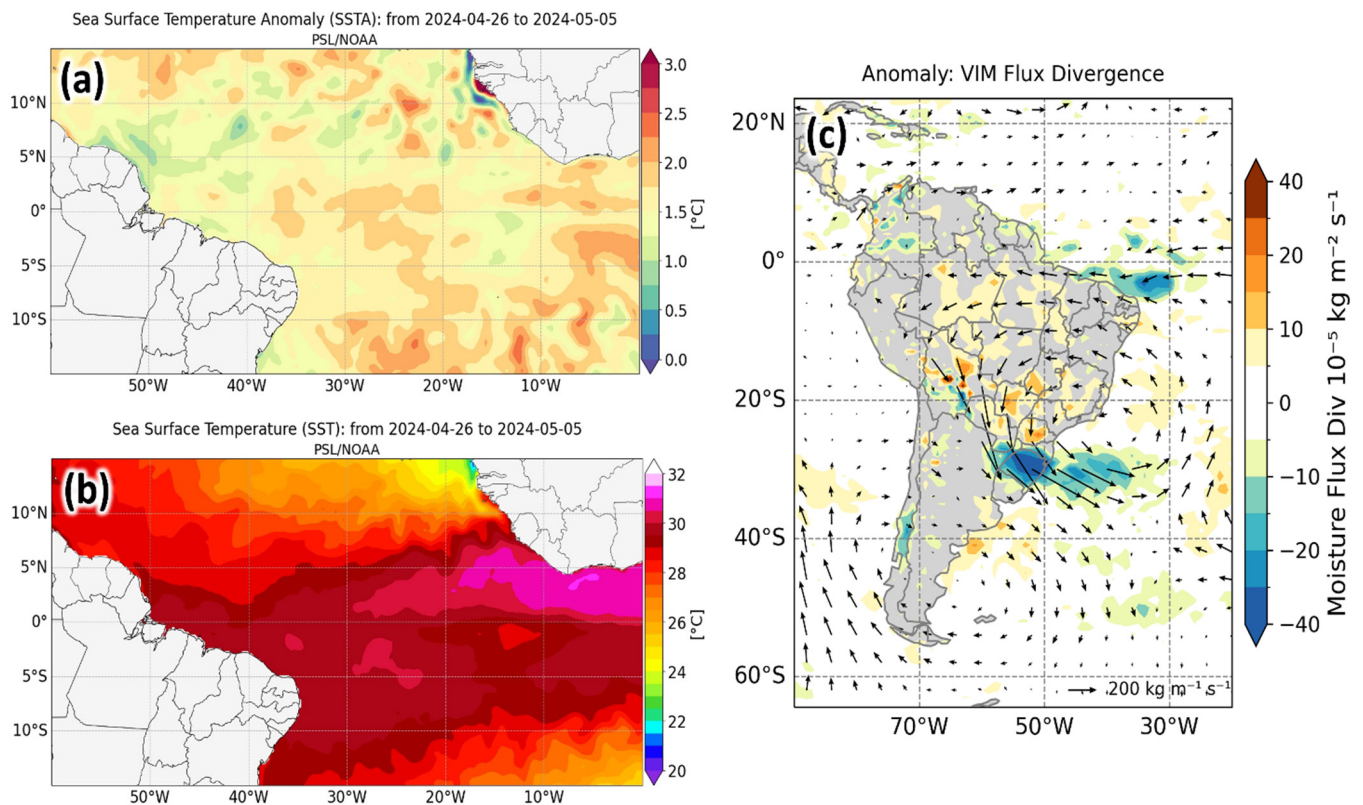


Figure 14. (a) Anomaly and (b) average of the sea surface temperature (°C) from 26 April to 5 May 2024, and (c) anomalies of the vertically integrated moisture flux divergence (shaded; $10^{-5} \text{ kg m}^{-2} \text{ s}^{-1}$) and vertically integrated moisture flux vectors ($\text{kg m}^{-1} \text{ s}^{-1}$) between 1000 hPa and 200 hPa. Anomalies were obtained by subtracting the climatology averaged over April and May from 1980 to 2023 from the average for 26 April to 5 May 2024.

The analysis of moisture flux divergence reveals that the anomalous circulation of the SASA transported moisture from the Atlantic to the northern region of Brazil. Subsequently, this moisture was directed to the country's south through the LLJ. It is important to highlight that the Amazon Basin plays a crucial role in recycling this moisture from the Atlantic due to the intense evapotranspiration process in the region. Finally, negative values

of moisture divergence over the RS indicate regions of strong moisture convergence in the LLJ exit area (Figure 14c).

3.4. Mesoscale

Figure 15 presents the spatial distribution of precipitation, soil moisture, and total lightning registered between 26 April and 5 May 2024. During this period, precipitation (above 50 mm) covered the whole state of RS (Figure 15a,b). However, higher precipitation volumes (>400 mm) were concentrated in the central-northern part of the state, which also registered the higher precipitation volume by the rain gauges (Figure 1). Although MERGE presented higher precipitation than CHIRPS (>600 mm versus ~550 mm), both products presented similar spatial patterns for precipitation. Indeed, as demonstrated by several studies [65–67], MERGE typically shows higher correlations and lower errors than the CHIRPS product when compared with rain gauges.

The large area covered by precipitation is a consequence of the development of several MCSs. This result is consistent with those shown in Figure 13, which reveal the presence of MCSs covering most of RS with lower brightness temperatures (< -85 °C). This finding aligns with previous studies by Durkee and Mote [68] and Durkee et al. [69], highlighting the essential contribution of MCSs to precipitation across subtropical South America. Additionally, MCSs maintain favorable conditions for tornadoes. In fact, some tornadoes were reported by PREVOTS during the studied extreme event. One tornado was registered at São Martinho da Serra City (western part of RS State) on 27 April at 2000 UTC and another at Gentil City (northern part of RS State) on 11 May 2024 at 1650 using camera images from a video that recorded the event (Figures 1 and 2e,f). Previous works on Brazil have documented tornadoes related to supercell and MCS characteristics [70–72].

Regarding soil moisture at the surface (Figure 15c), the fraction volume is above 0.3 for the entire state of RS. Additionally, for the central-northern part of the state, values above 0.55 were observed. These results are consistent with the precipitation maps (Figure 15a,b), indicating very moist soil, yielding favorable conditions for the occurrence of landslides. Figure 3c shows that the soil moisture had been increasing since the beginning of April. These results are consistent with de Freitas et al. [48], which showed the importance of the persistence of higher soil moisture for disaster occurrence.

During the analyzed period (from 26 April to 5 May), the total lightning observed by GOES-16 occurred in the entire state of RS, with higher (>10 flashes km^{-2} in 10 days) occurrence in the central-northern part of the state. A similar distribution was observed for precipitation (Figure 15a,b). Oda et al. [73] showed that the average lightning density in this region is approximately 25–30 flashes $\text{km}^2 \text{ year}^{-1}$, indicating that this storm produced $1/3$ of the total lightning expected for the entire year. These results indicate anomalous lightning activity during these periods caused by several mesoscale thunderstorms.

Figure 16 presents the CAPPI images of reflectivity at a 2 km height from the Santiago weather radar. Several storms were observed in the central-eastern-southern part of RS State for several days, indicating a persistent occurrence of precipitating clouds. Reflectivity values higher than 55 dBZ were observed in several regions. As reflectivity is related to the number of hydrometeors and the sixth power of the particle diameter [74], these results indicate the existence of higher concentrations of large raindrops. These observations are consistent with the higher precipitation volume observed in the earlier results (Figures 3 and 15). In addition, Figure 16 is consistent with Figure 1a. On the east side of the radar, several storms and natural disasters (six floods and three landslides) were observed.

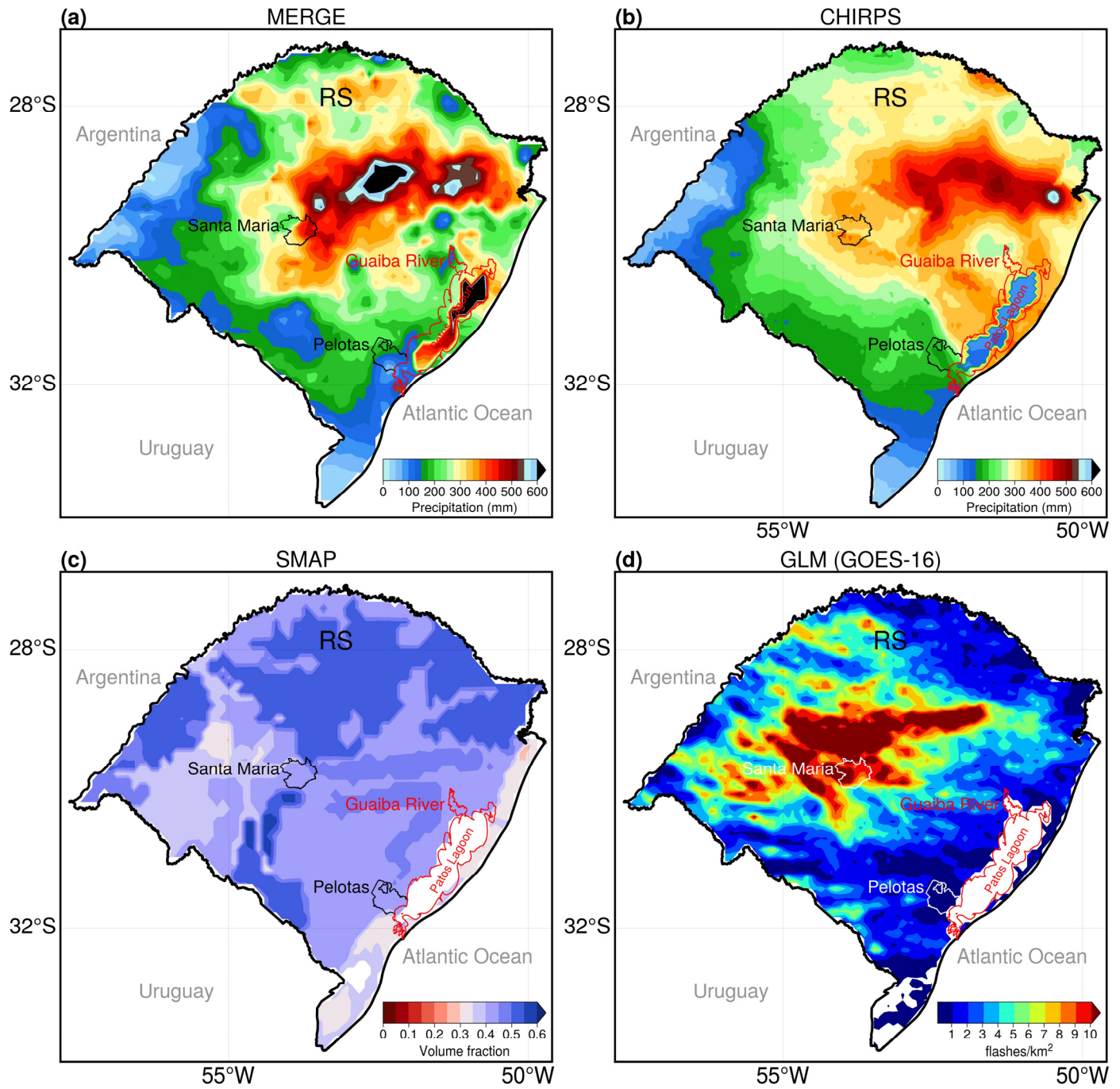


Figure 15. (a,b) Accumulated precipitation (mm) estimated from MERGE and CHIRPS, (c) maximum soil moisture (volume fraction) from SMAP, and (d) accumulated total lightning flash (flashes/km²) from GLM aboard GOES-16 satellite from 26 April to 5 May 2024.

Figure 17 presents the CAPPI reflectivity at a 2 km height and vertical cross-section on 27 April 2024 at 1950, 2000, and 2010 UTC, representing the closest times to the São Martinho da Serra tornado. The tornado occurred close to the border of a straight-line storm that presented several convective cells embedded with higher reflectivity values (up to 60 dBZ) (Figure 17a,c,e). For the vertical cross-section (Figure 17b), the horizontal size of the storm is approximately 21 km, and the tornado occurred close to a convective cell with higher (up to 60 dBZ) reflectivity and a size of approximately 8 km. This core extends beyond 7.5 km of height, representing an isotherm's location of approximately -10°C . As observed by Pereira et al. [75], this region inside the clouds is prone to strong updrafts and

lightning formation. These results are consistent with this region’s higher precipitation volume and lightning occurrence.

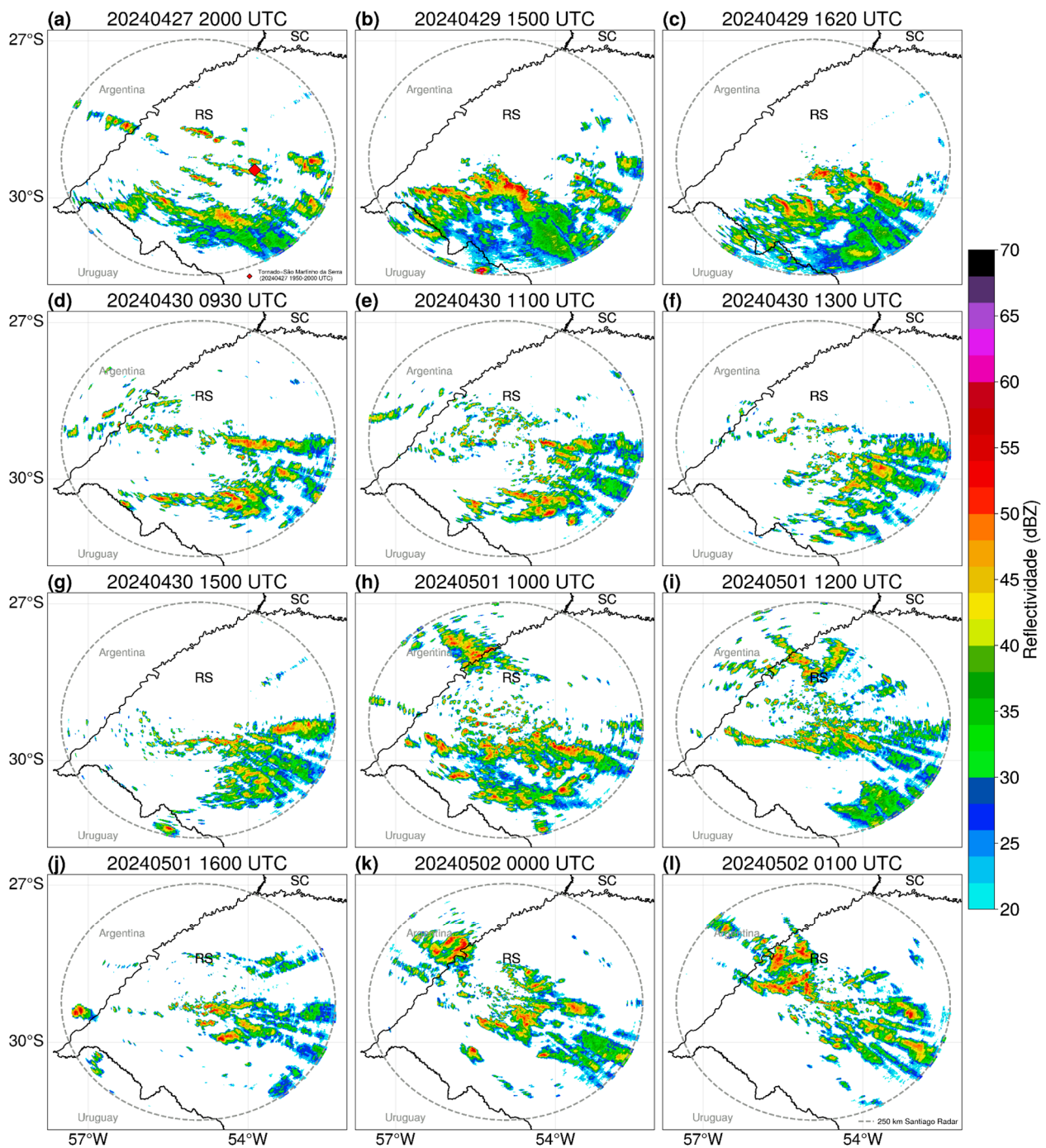


Figure 16. (a–l) Constant Plan Position Indicator (CAPPI) at 2 km height of reflectivity from Santiago weather radar (RS) from 27 April at 2000 UTC to 2 May at 0100 UTC.

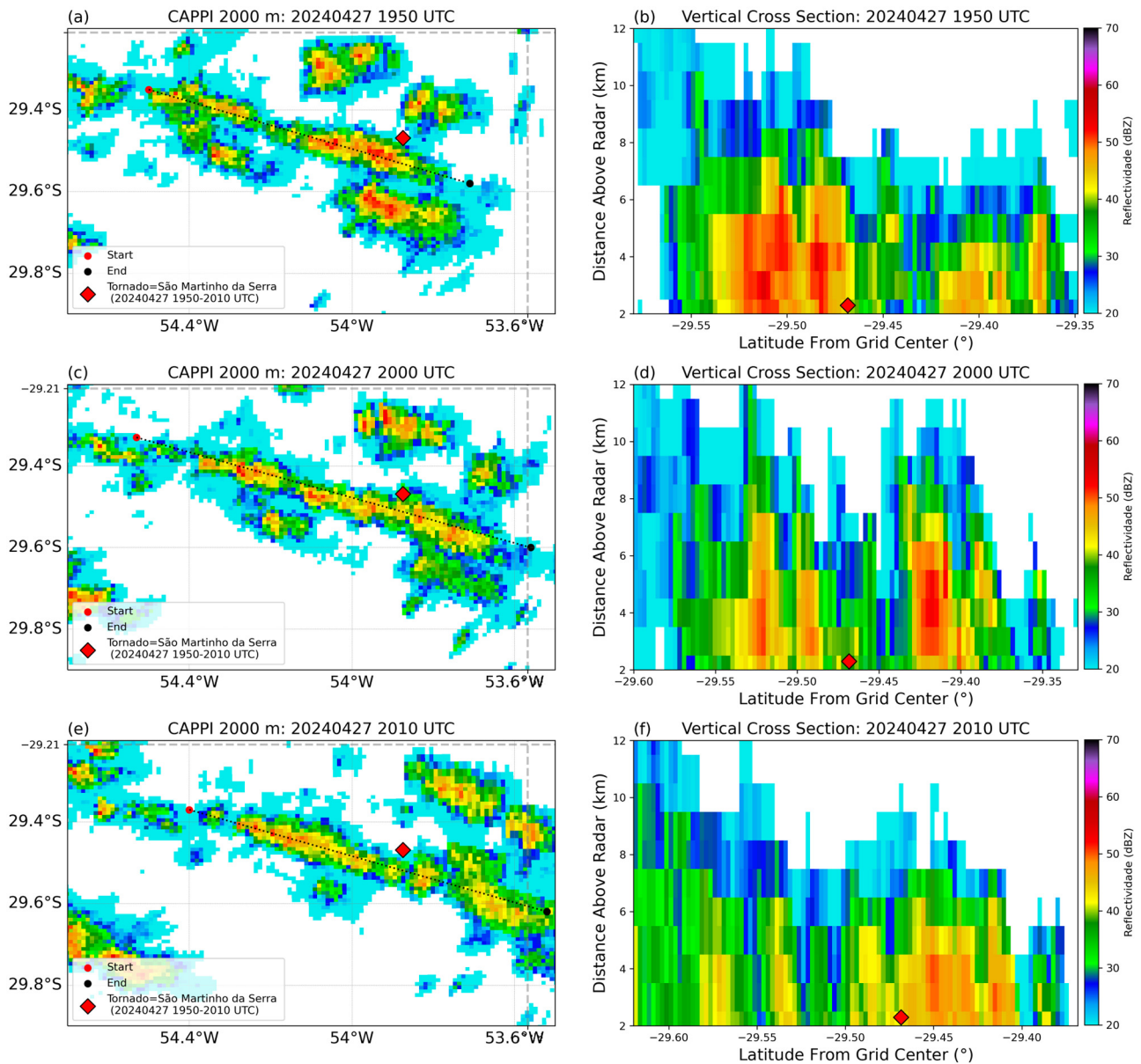


Figure 17. CAPPI at 2 km height of reflectivity and vertical transversal section of a thunderstorm from Santiago radar on 27 April at (a,b) 1950, (c,d) 2000, and (e,f) 2020 UTC. The dashed line in figures (a,c,e) represents the vertical transversal section, and the red diamond is the location of the São Martinho da Serra tornado.

4. Conclusions

This study provides a comprehensive multi-scale analysis of the extreme event of precipitation that occurred in RS (southern Brazil) from 26 April to 5 May 2024. This extreme event produced 70 natural disasters (8 floodings, 39 floods, 18 landslides, 4 flash floods, and 1 rockfall) in 10 days (according to the CEMADEN), at least one tornado (on 27 April 2024) during this period, and associated precipitation amounts that exceeded the climatology for April and May three times. These disasters directly affected 2,398,255 people, leading to 183 deaths. This episode is distinct from others that have occurred in RS or other regions around the globe mainly because of the large-scale drivers that triggered the precipitating atmospheric systems, as well as the physical peculiarities of the area. The main findings are summarized below:

Large scale: On a large scale, a teleconnection pattern originating from the Indian Ocean favored an anomalous barotropic high-pressure pattern over central-southeastern

Brazil. At upper levels, this pattern contributed to increasing the speed of westerly winds (subtropical jet) and, at the surface, the north-northwest winds (low-level jet east of the Andes).

Synoptic scale: The strengthened subtropical jet contributed as an air-uplifting mechanism and was associated with the warm and moist air transported by the low-level jet east of the Andes, which led to the formation of mesoscale convective systems. The passage of a cold front on 28 April also contributed to the heavy rains that affected RS.

Mesoscale: The synoptic environment triggered the formation of several MCSs with deep clouds (temperatures decreased to -85° , as viewed by satellite estimates, which caused a higher precipitation volume). The storms produced higher precipitation (>400 mm in 10 days) and total lightning (>10 flashes km^{-2}) in the central-eastern part of RS State. The lightning registered represents one-third of the lightning expected for the entire year. This precipitation pattern promoted higher soil moisture, reaching a 0.5 volume fraction. The higher precipitation volume, the higher volume of rivers, and soil saturation were probably fundamental factors in producing these natural disasters. Regarding the weather radar, several convective cells were observed moving from west to east on the Santiago radar with high reflectivity values (> 50 dBZ). The tornado registered at São Martinho da Serra on 27 April 2024 between 1950 and 2010 UTC was associated with a deep precipitating system, which presented deep columns with higher reflectivity (60 dBZ) up to 7 km in height.

This study does not discuss the societal impacts of this extreme event. Still, it deserves future attention to highlight the region's vulnerability and the fragility of the public politics of RS State. For future studies, an investigation of the implementation of risk management and urban expansion plans for cities in RS State is recommended. It is crucial to emphasize the need for enhanced communication between institutions and the public and improvements in monitoring and alert systems. For instance, expanding the network of meteorological stations and weather radars, alongside training technical personnel in weather forecasting, is essential. Investing in state and regional meteorological centers is pivotal for mitigating the impacts of natural disasters. Furthermore, increasing investment capital and establishing a robust resource allocation and utilization framework are central to this effort. In this regard, it is imperative to channel resources effectively into high-quality infrastructure projects that consider the potential impacts projected by climate change.

Author Contributions: Conceptualization, M.S.R., E.V.M. and B.C.C.; methodology, M.S.R., E.V.M., B.C.C. and D.O.d.S.; software, M.S.R., E.V.M., D.O.d.S. and B.C.C.; formal analysis, M.S.R., E.V.M., D.O.d.S. and B.C.C.; writing—original draft preparation, M.S.R., E.V.M. and B.C.C.; writing—review and editing, M.S.R. and G.W.d.S.F. All authors have read and agreed to the published version of the manuscript.

Funding: The authors thank the Coordination for the Improvement of Higher Education Personnel (CAPES, Finance Code 001), the National Council for Scientific and Technological Development (CNPq), and the Research Supporting Foundation of Minas Gerais State (FAPEMIG).

Institutional Review Board Statement: Not applicable.

Informed Consent Statement: Not applicable.

Data Availability Statement: All datasets used in this study are available from public online databases (links are provided in the methodology section).

Acknowledgments: The authors thank all the meteorological centers that provided the data used in this study.

Conflicts of Interest: Author Bruno César Capucin was employed by the company Ampere Consultoria. The remaining authors declare that the research was conducted in the absence of any commercial or financial relationships that could be construed as a potential conflict of interest.

References

1. Regoto, P.; Dereczynski, C.; Chou, S.C.; Bazzanella, A.C. Observed changes in air temperature and precipitation extremes over Brazil. *Int. J. Climatol.* **2021**, *41*, 5125–5142. [[CrossRef](#)]

2. Reboita, M.S.; da Rocha, R.P.; Souza, C.A.D.; Baldoni, T.C.; Silva, P.L.L.D.S.; Ferreira, G.W.S. Future projections of extreme precipitation climate indices over South America based on CORDEX-CORE multimodel ensemble. *Atmosphere* **2022**, *13*, 1463. [CrossRef]
3. Faria, L.F.; Reboita, M.S.; Mattos, E.V.; Carvalho, V.S.B.; Martins Ribeiro, J.G.; Capucin, B.C.; Drumond, A.; Paes dos Santos, A.P. Synoptic and mesoscale analysis of a severe weather event in Southern Brazil at the end of June 2020. *Atmosphere* **2023**, *14*, 486. [CrossRef]
4. Alcântara, E.; Marengo, J.A.; Mantovani, J.; Londe, L.R.; San, R.L.Y.; Park, E.; Lin, Y.N.; Wang, J.; Mendes, T.; Cunha, A.; et al. Deadly disasters in southeastern South America: Flash floods and landslides of February 2022 in Petrópolis, Rio de Janeiro. *Nat. Hazards Earth Syst. Sci.* **2023**, *23*, 1157–1175. [CrossRef]
5. Bartolomei, F.R.; Ribeiro, J.G.M.; Reboita, M.S. Eventos Extremos de Precipitação no Sudeste do Brasil: Verão 2021/2022. *Rev. Bras. Geo. Fis.* **2023**, *16*, 2658–2676. [CrossRef]
6. Oda, P.S.S.; Teixeira, D.L.S.; Pinto, T.A.C.; da Silva, F.P.; Riondet-Costa, D.R.T.; Mattos, E.V.; de Souza, D.O.; Bartolomei, F.; Reboita, M.S.; Santos, A.P.P.D. Disasters in Petrópolis, Brazil: Political, urban planning, and geometeorological factors that contributed to the event on February 15, 2022. *Urban Clim.* **2024**, *4*, 101849. [CrossRef]
7. Marengo, J.A.; Cunha, A.P.; Seluchi, M.E.; Camarinha, P.I.; Dolif, G.; Sperling, V.B.; Alcântara, E.H.; Ramos, A.M.; Andrade, M.M.; Stabile, R.A.; et al. Heavy rains and hydrogeological disasters on February 18th–19th, 2023, in the city of São Sebastião, São Paulo, Brazil: From meteorological causes to early warnings. *Nat. Hazards* **2024**, *120*, 7997–8024. [CrossRef]
8. Bartolomei, F.R.; Reboita, M.S.; da Rocha, R.P. Ciclones extratropicais causadores de eventos extremos no sul do Brasil no inverno de 2023. *Terrae Didactica* **2024**, *20*, e024003. [CrossRef]
9. Mantovani, J.; Alcântara, E.; Pampuch, L.A.; Baião, C.F.P.; Park, E.; Custódio, M.S.; Gozzo, L.F.; Bortolozzo, C.A. Assessing flood risks in the Taquari-Antas Basin (Southeast Brazil) during the September 2023 extreme rainfall surge. *Nat. Hazards* **2024**, *1*, 9. [CrossRef]
10. United Nations. Brazil Floods: UNHCR—WMO. Available online: <https://www.unognewsroom.org/story/en/2183/brazil-floods-unhcr-wmo> (accessed on 27 August 2024).
11. British Broadcasting Corporation (BBC). Foi Assustador: Carta de 83 Anos Detalha Estragos da Grande Enchente de 1941 no Rio Grande do Sul. Available online: <https://www.bbc.com/portuguese/articles/c2898rxg1j9o#:~:text=Na%20enchente%20de%20maio%20de,dias%20de%20chuvas%20naquele%20m%C3%AAs> (accessed on 26 May 2024).
12. Agência Nacional de Águas e Saneamento Básico (ANA). Cais Mauá C6. Available online: <https://app.powerbi.com/view?r=eyJrJoiZTRjZDlmYjgtNzAzMS00ZTFmLTlmZDA0tNzEwNjM0MDU0NTJhIiwidCI6ImUwYmI0MDEyLTgxMGItNDY5YS04YjRkLTY2N2ZjZDFiYWY4OCJ9> (accessed on 31 May 2024).
13. Defesa Civil. Defesa Civil Atualiza Balanço das Enchentes no RS-9/8. Available online: <https://defesacivil.rs.gov.br/defesa-civil-atualiza-balanco-das-enchentes-no-rs-10-7-66b67813ba21f> (accessed on 10 September 2024).
14. Blunden, J.; Boyer, T. State of the climate in 2023. *Bull. Amer. Meteor. Soc.* **2024**, *105*, S1–S484. [CrossRef]
15. United Nations Office for the Coordination of Humanitarian Affairs (OCHA). Annual Report 2023. Available online: https://reliefweb.int/attachments/03b7230c-6890-478c-bacf-2f627caa908f/OCHA_Annual_Report_2023.pdf?_gl=1*zwywdo*_ga*MTcyODY2MDY0OS4xNzI0NzIzZjYy*_ga_E60ZNX2F68*MTcyNDgzMzU5My4zLjEuMTcyNDgzMzYyNi4yNy4wLjA (accessed on 1 June 2024).
16. Suertegaray, D.M.A.; Fujimoto, N.S.V.M. Morfogenese do Relevo do Estado do Rio Grande do Sul. In *Rio Grande do Sul: Paisagens e Territórios em Transformação*, 2nd ed.; Verdum, R., Basso, L.A., Suertegaray, D.M.A., Eds.; Editora da UFRGS: Porto Alegre, Brasil, 2012; pp. 11–26. Available online: <https://lume.ufrgs.br/bitstream/handle/10183/218530/000869820.pdf?sequence=1&isAllowed=y> (accessed on 25 May 2024).
17. Kottke, M.; Grieser, J.; Beck, C.; Rudolf, B.; Rubel, F. World map of the Köppen–Geiger climate classification updated. *Meteorol. Z.* **2006**, *15*, 259–263. [CrossRef] [PubMed]
18. Ferreira, G.W.S.; Reboita, M.S. A new look into the South America precipitation regimes: Observation and forecast. *Atmosphere* **2022**, *13*, 873. [CrossRef]
19. Instituto Nacional de Meteorologia (INMET). Normais Climatológicas do Brasil. Available online: <https://portal.inmet.gov.br/normais> (accessed on 31 August 2024).
20. G1. Resgate do Cavalo Caramelo: Entenda Como Animal foi Retirado de Telhado no RS. Available online: <https://g1.globo.com/rs/rio-grande-do-sul/noticia/2024/05/09/resgate-do-cavalo-caramelo-entenda-como-animal-foi-retirado-de-cima-do-telhado-no-rs.ghtml> (accessed on 31 May 2024).
21. PREVOTS. Available online: www.prevots.org/ (accessed on 31 August 2024).
22. Ribeiro, B.; Schild, G.; Santos, L.; Nascimento, E.L.; Lopes, M.; Goede, V.; dos Santos, L.D.O.; Costa, I.; Ferreira, V.; Oliveira, M.; et al. The Brazilian Severe Storm Reports Database: Methodology and a Preliminary Climatology. In Proceedings of the Climatologies of Severe Storms and Their Environments, Santa Fe, NM, USA, 27 October 2022; American Meteorological Society: Boston, MA, USA, 2022. Available online: <https://ams.confex.com/ams/30SLS/meetingapp.cgi/Paper/407158> (accessed on 2 September 2024).
23. Centro Nacional de Monitoramento e Alertas de Desastres Naturais (CEMADEN). Mapa Interativo da Rede Observacional Para Monitoramento de Risco de Desastres Naturais do Cemaden. Available online: <https://mapainterativo.cemaden.gov.br/> (accessed on 1 June 2024).

24. Correio Braziliense. Após Inundações, Infraestrutura do Rio Grande do Sul Está Comprometida. Available online: <https://www.correio braziliense.com.br/brasil/2024/05/6850774-apos-inundacoes-infraestrutura-do-rio-grande-do-sul-esta-comprometida.html> (accessed on 31 May 2024).
25. Agência Brasil. Mais de 78% dos Municípios Gaúchos Foram Impactados Pelas Chuvas. Available online: <https://agenciabrasil.ebc.com.br/geral/noticia/2024-05/mais-de-78-dos-municipios-gauchos-foram-impactados-pelas-chuvas> (accessed on 29 May 2024).
26. Jovem Pan. Sobe para 83 o Número de Mortos no Rio Grande do Sul. Available online: <https://jovempan.com.br/noticias/brasil/sobe-para-83-o-numero-de-mortos-no-rio-grande-do-sul.html> (accessed on 29 May 2024).
27. O Globo. Tragédia no RS e até Resgate de Cavalo Caramelo Viram Pano de Fundo para Polarização Política. Available online: <https://oglobo.globo.com/brasil/sos-rio-grande-do-sul/noticia/2024/05/09/tragedia-no-rs-e-ate-resgate-de-cavalo-caramelo-viram-pano-de-fundo-para-polarizacao-politica.ghtml> (accessed on 29 May 2024).
28. UOL. Vídeo Mostra Passagem de Tornado no Interior do Rio Grande do Sul; Veja. Available online: <https://noticias.uol.com.br/videos/2024/04/28/video-mostra-passagem-de-tornado-no-interior-do-rio-grande-do-sul-veja.htm> (accessed on 29 August 2024).
29. UOL. Rio Grande do Sul: Tornado Atinge Gentil (RS) e Destelha Casas; Veja Vídeo. Available online: <https://noticias.uol.com.br/videos/2024/05/11/rio-grande-do-sul-tornado-atinge-gentil-rs-e-destelha-casas-veja-video.htm> (accessed on 29 August 2024).
30. Hersbach, H.; Bell, B.; Berrisford, P.; Hirahara, S.; Horányi, A.; Muñoz-Sabater, J.; Nicolas, J.; Peubey, C.; Radu, R.; Schepers, D.; et al. The ERA5 global reanalysis. *Q. J. R. Meteorol. Soc.* **2020**, *146*, 1999–2049. [CrossRef]
31. National Oceanic and Atmospheric Administration (NOAA). OI SST V2 High Resolution Dataset. Available online: <https://psl.noaa.gov/data/gridded/data.noaa.oisst.v2.highres.html> (accessed on 1 June 2024).
32. National Oceanic and Atmospheric Administration (NOAA). Climate Prediction Center (CPC) Daily Blended Outgoing Longwave Radiation (OLR)-2.5 Degree. Available online: https://psl.noaa.gov/data/gridded/data.cpc_blended_olr-2.5deg.html (accessed on 1 June 2024).
33. Souza, C.A.; Reboita, M.S. Ferramenta para o monitoramento dos padrões de teleconexão na América do Sul. *Terræ Didat.* **2021**, *17*, e021009. [CrossRef]
34. Índices de Teleconexões. Available online: <https://meteorologia.unifei.edu.br/teleconexoes/> (accessed on 1 June 2024).
35. Geostationary Operational Environmental Satellite (GOES-16) Satellite. Available online: <https://ftp.cptec.inpe.br/goes/goes16/retangular/ch13/> (accessed on 1 June 2024).
36. Observing Systems Capability Analysis and Review Tool (OSCAR). Available online: https://space.oscar.wmo.int/satellites/view/goes_16 (accessed on 30 June 2024).
37. Goodman, S.J.; Blakeslee, R.J.; Koshak, W.J.; Mach, D.; Bailey, J.; Buechler, D.; Carey, L.; Schultz, C.; Bateman, M.; McCaul, E.; et al. The GOES-R Geostationary Lightning Mapper (GLM). *Atmos. Res.* **2013**, *125–126*, 34–49. [CrossRef]
38. GOES-R Geostationary Lightning Mapper (GLM)–Amazon AWS. Available online: <https://noaa-goes16.s3.amazonaws.com/index.html#GLM-L2-LCFA/> (accessed on 30 June 2024).
39. GOES-R Geostationary Lightning Mapper (GLM) Acumulado. Available online: http://ftp.cptec.inpe.br/goes/goes16/goes16_web/glm_acumulado_nc/ (accessed on 30 June 2024).
40. Rozante, J.R.; Moreira, D.S.; Gonçalves, L.G.G.; Vila, D.A. Combining TRMM and surface observations of precipitation: Technique and validation over South America. *Weather Forecast.* **2010**, *25*, 885–894. [CrossRef]
41. MERGE–GPM. Available online: <https://ftp.cptec.inpe.br/modelos/tempo/MERGE/GPM/> (accessed on 30 June 2024).
42. Funk, C.; Peterson, P.; Landsfeld, M.; Pedreros, D.; Verdin, J.; Shukla, S.; Husak, G.; Rowland, J.; Harrison, L.; Hoell, A.; et al. The climate hazards infrared precipitation with stations—a new environmental record for monitoring extremes. *Sci. Data* **2015**, *2*, 150066. [CrossRef]
43. CHIRPS Daily: Climate Hazards Center InfraRed Precipitation with Station Data (Version 2.0 Final). Available online: https://developers.google.com/earth-engine/datasets/catalog/UCSB-CHG_CHIRPS_DAILY (accessed on 30 June 2024).
44. Soil Moisture Active–Passive (SMAP). Available online: <https://smap.jpl.nasa.gov/> (accessed on 30 June 2024).
45. SPL4SMGP.007 SMAP L4 Global 3-Hourly 9-km Surface and Root Zone Soil Moisture. Available online: https://developers.google.com/earth-engine/datasets/catalog/NASA_SMAP_SPL4SMGP_007 (accessed on 30 June 2024).
46. Peixoto, J.P.; Oort, A.H. *Physics of Climate*; American Institute of Physics: New York, NY, USA, 1992; 520p.
47. Kidder, S.Q.; Haar, T.H.V. *Satellite Meteorology: An Introduction*; Academic Press: Cambridge, MA, USA, 1995; 466p.
48. de Freitas, A.A.; Oda, P.S.S.; Teixeira, D.L.S.; Silva, P.N.; Mattos, E.V.; Bastos, I.R.P.; Nery, T.D.; Metodiev, D.; Santos, A.P.P.D.; Gonçalves, W.A. Meteorological conditions and social impacts associated with natural disaster landslides in the Baixada Santista region from March 2nd–3rd, 2020. *Urban Clim.* **2022**, *42*, 101110. [CrossRef]
49. Reynolds, S.E.; Brook, M.; Gourley, M.F. Thunderstorm charge separation. *J. Atmos. Sci.* **1957**, *14*, 426–436. [CrossRef]
50. Takahashi, T. Riming electrification as a charge generation mechanism in thunderstorms. *J. Atmos. Sci.* **1978**, *35*, 1536–1548. [CrossRef]
51. Instituto Nacional de Meteorologia (INMET). Eventos Extremos de Maio de 2024 no Brasil. Available online: <https://portal.inmet.gov.br/uploads/notastecnicas/EventosExtremos-Brasil-Maio-2024.pdf> (accessed on 1 September 2024).
52. Oceanic Niño Index (ONI). Available online: <https://meteorologia.unifei.edu.br/teleconexoes/indice?id=oni> (accessed on 30 June 2024).

53. Reboita, M.S.; Ambrizzi, T.; Crespo, N.M.; Dutra, L.M.M.; Ferreira, G.W.S.; Rehbein, A.; Drumond, A.; da Rocha, R.P.; de Souza, C.A. Impacts of teleconnection patterns on South America climate. *Ann. N. Y. Acad. Sci.* **2021**, *1504*, 116–153. [[CrossRef](#)] [[PubMed](#)]
54. Taschetto, A.S.; Ambrizzi, T. Can Indian Ocean SST anomalies influence South American rainfall? *Clim. Dyn.* **2012**, *38*, 1615–1628. [[CrossRef](#)]
55. Agência Brasil. Chuvas na África Deixam pelo Menos 473 Mortos e 1,6 Milhão de Afetados. Available online: [\(https://agenciabrasil.ebc.com.br/internacional/noticia/2024-05/chuvas-na-africa-deixam-pelo-menos-473-mortos-e-16-milhao-de-afetados#:~:text=Pelo%20menos%20473%20pessoas%20morreram,das%20Na%C3%A7%C3%B5es%20Unidas%20\(ONU\)\)](https://agenciabrasil.ebc.com.br/internacional/noticia/2024-05/chuvas-na-africa-deixam-pelo-menos-473-mortos-e-16-milhao-de-afetados#:~:text=Pelo%20menos%20473%20pessoas%20morreram,das%20Na%C3%A7%C3%B5es%20Unidas%20(ONU)) (accessed on 4 June 2024).
56. National Oceanic and Atmospheric Administration (NOAA). Madden-Julian Oscillation: Recent Evolution, Current Status and Predictions. Available online: <https://www.cpc.ncep.noaa.gov/products/precip/CWlink/MJO/mjoupdate.pdf> (accessed on 26 May 2024).
57. Karoly, D.J. Southern Hemisphere circulation features associated with El Niño-Southern Oscillation events. *J. Clim.* **1989**, *2*, 1239–1252. [[CrossRef](#)]
58. Trenberth, K.E.; Branstator, G.W.; Karoly, D.; Kumar, A.; Lau, N.-C.; Ropelewski, C. Progress during TOGA in understanding and modeling global teleconnections associated with tropical sea surface temperatures. *J. Geophys. Res.* **1998**, *103*, 14291–14324. [[CrossRef](#)]
59. Ambrizzi, T.; Hoskins, B.J. Stationary rossby-wave propagation in a baroclinic atmosphere. *Q. J. R. Meteorol. Soc.* **1997**, *123*, 919–928. [[CrossRef](#)]
60. Nascimento, E.L.; Ambrizzi, T. The influence of atmospheric blocking on the rossby wave propagation in the southern hemisphere winter flows. *J. Meteorol. Soc. Jpn.* **2002**, *80*, 139–159. [[CrossRef](#)]
61. Zhao, S.; Li, J.; Li, Y.; Jin, F.-F.; Zheng, J. Interhemispheric influence of Indo-Pacific convection oscillation on Southern Hemisphere rainfall through southward propagation of Rossby waves. *Clim. Dyn.* **2019**, *52*, 3203–3221. [[CrossRef](#)]
62. Reboita, M.S.; Ambrizzi, T.; Silva, B.A.; Pinheiro, R.F.; da Rocha, R.P. The South Atlantic subtropical anticyclone: Present and future climate. *Front. Earth Sci.* **2019**, *7*, 8. [[CrossRef](#)]
63. Silva Dias, M.A.F.D. Sistemas de mesoescala e previsão de tempo a curto prazo. *Rev. Bras. Meteorol.* **1987**, *2*, 133–150.
64. Martinez, D.M.; Solman, S.A. Synoptic patterns associated with extreme precipitation events over southeastern South America during spring and summer seasons. *Int. J. Climatol.* **2022**, *42*, 10387–10406. [[CrossRef](#)]
65. Rozante, J.R.; Gutierrez, E.R.; Fernandes, A.A.; Vila, D.A. Performance of precipitation products obtained from combinations of satellite and surface observations. *Int. J. Remote Sens.* **2020**, *41*, 7585–7604. [[CrossRef](#)]
66. Cassalho, F.; Rennó, C.D.; Reis, J.B.C.; Silva, B.C. Hydrologic validation of MERGE precipitation products over anthropogenic watersheds. *Water* **2020**, *12*, 1268. [[CrossRef](#)]
67. Silva, E.H.L.; Silva, F.D.S.; Silva Junior, R.S.; Pinto, D.D.C.; Costa, R.L.; Gomes, H.B.; Júnior, J.B.C.; de Freitas, I.G.F.; Herdies, D.L. Performance assessment of different precipitation databases (gridded analyses and reanalyses) for the new Brazilian agricultural frontier: SEALBA. *Water* **2022**, *14*, 1473. [[CrossRef](#)]
68. Durkee, J.D.; Mote, T.L. A climatology of warm-season mesoscale convective complexes in subtropical South America. *Int. J. Climatol.* **2010**, *30*, 418–431. [[CrossRef](#)]
69. Durkee, J.D.; Mote, T.L.; Shepherd, J.M. The contribution of mesoscale convective complexes to rainfall across subtropical South America. *J. Clim.* **2009**, *22*, 4590–4605. [[CrossRef](#)]
70. Silva Dias, M.A.F. An increase in the number of tornado reports in Brazil. *Wea. Clim. Soc.* **2011**, *3*, 209–217. [[CrossRef](#)]
71. Nascimento, E.D.L.; Held, G.; Gomes, A.M. A multiple-vortex tornado in southeastern Brazil. *Mon. Weather Rev.* **2014**, *142*, 3017–3037. [[CrossRef](#)]
72. Ferreira, V.; Goede, V.; Nascimento, E.L. An environmental and polarimetric study of the 19 November 2015 supercell and multiple-vortex tornado in Marechal Cândido Rondon, southern Brazil. *Meteor. Atmos. Phys.* **2022**, *134*, 82. [[CrossRef](#)]
73. Oda, P.S.S.; Enoré, D.P.; Mattos, E.V.; Gonçalves, W.A.; Albrecht, R.I. An initial assessment of the distribution of total Flash Rate Density (FRD) in Brazil from GOES-16 Geostationary Lightning Mapper (GLM) observations. *Atmos. Res.* **2022**, *270*, 106081. [[CrossRef](#)]
74. Rinehart, R.E. *Radar for Meteorologists*, 5th ed.; Rinehart Publications: New York, NY, USA, 2010; 482p.
75. Pereira, R.G.; Ribeiro, J.G.M.; Mattos, E.V.; Reboita, M.S. Analysis of a hailstorm in the south of Minas Gerais state on October 13, 2020. *Meteorol. Atmos. Phys.* **2024**, *136*, 21. [[CrossRef](#)]

Disclaimer/Publisher’s Note: The statements, opinions and data contained in all publications are solely those of the individual author(s) and contributor(s) and not of MDPI and/or the editor(s). MDPI and/or the editor(s) disclaim responsibility for any injury to people or property resulting from any ideas, methods, instructions or products referred to in the content.